MEMORANDUM REPORT ARBRL-MR-03232

COMPARISON OF HULL HYDROCODE COMPUTATIONS OF SHOCK TUBE BLOCKAGE EFFECTS ON TARGET LOADING FOR STEP SHOCKS AND RAPIDLY-DECAYING SHOCKS

John D. Wortman
Richard E. Lottero

December 1982

US ARMY ARMAMENT RESEARCH AND DEVELOPMENT COMMAND
BALLISTIC RESEARCH LABORATORY
ABERDEEN PROVING GROUND, MARYLAND

Destroy this report when it is no longer needed.
Do not return it to the originator.

Secondary distribution of this report is prohibited.

Additional copies of this report may be obtained from the National Technical Information Service, U. S. Department of Commerce, Springfield, Virginia 22161.

The findings in this report are not to be construed as an official Department of the Army position, unless so designated by other authorized documents.

The use of trade names or manufacturers' names in this report does not constitute indorsement of any commercial product.

UNCLASSIFIED
SECURITY CLASSIFICATION OF THIS PAGE *(When Data Entered)*

REPORT DOCUMENTATION PAGE

READ INSTRUCTIONS BEFORE COMPLETING FORM

1. REPORT NUMBER: Memorandum Report ARBRL-MR-03232
2. GOVT ACCESSION NO.:
3. RECIPIENT'S CATALOG NUMBER:

4. TITLE *(and Subtitle)*: Comparison of HULL Hydrocode Computations of Shock Tube Blockage Effects on Target Loading for Step Shocks and Rapidly-Decaying Shocks

5. TYPE OF REPORT & PERIOD COVERED: Final Report August 1981 - August 1982

6. PERFORMING ORG. REPORT NUMBER:

7. AUTHOR(s): John D. Wortman and Richard E. Lottero

8. CONTRACT OR GRANT NUMBER(s):

9. PERFORMING ORGANIZATION NAME AND ADDRESS:
US Army Ballistic Research Laboratory
ATTN: DRDAR-BLT
Aberdeen Proving Ground, MD 21005

10. PROGRAM ELEMENT, PROJECT, TASK AREA & WORK UNIT NUMBERS:
1L162618AH25
1L162618AH80

11. CONTROLLING OFFICE NAME AND ADDRESS:
US Army Armament Research and Development Command
US Army Ballistic Research Laboratory (DRDAR-BL)
Aberdeen Proving Ground, MD 21005

12. REPORT DATE: December 1982

13. NUMBER OF PAGES: 50

14. MONITORING AGENCY NAME & ADDRESS *(if different from Controlling Office)*:

15. SECURITY CLASS. *(of this report)*: UNCLASSIFIED

15a. DECLASSIFICATION/DOWNGRADING SCHEDULE:

16. DISTRIBUTION STATEMENT *(of this Report)*:
Approved for public release; distribution unlimited

17. DISTRIBUTION STATEMENT *(of the abstract entered in Block 20, if different from Report)*:

18. SUPPLEMENTARY NOTES:

19. KEY WORDS *(Continue on reverse side if necessary and identify by block number)*:
shock tube blockage
HULL hydrocode
step shocks
decaying shocks
shock tube
blast simulator
blast loading

20. ABSTRACT *(Continue on reverse side if necessary and identify by block number)*:

The HULL hydrocode was used to make two-dimensional calculations (for the three-dimensional axisymmetric problem) of a rapidly-decaying shock wave striking a finite right-circular cylinder whose axis was coincident with that of a cylindrical shock tube. Calculations were made for three peak shock overpressures for 20 percent blockage and for a free-field encounter. These results were then compared with previously reported HULL computations for comparable

DD FORM 1 JAN 73 1473 EDITION OF 1 NOV 65 IS OBSOLETE

UNCLASSIFIED
SECURITY CLASSIFICATION OF THIS PAGE *(When Data Entered)*

overpressure step shocks for the same configuration. The net axial loading for these rapidly-decaying shocks behaved quite differently from that for the step shocks. It became negative early in the drag phase for the shock/target encounter in the free field, and oscillated about a net negative value in the drag phase. Net impulse showed a corresponding decrease (from a peak after the end of the diffraction phase) for the decaying shocks. Net impulse increased monotonically for the step shocks. Flow conditions in the constricted region were enhanced for the decaying shocks. Although the relative enhancement at late time was large compared with values for the same decaying-shock/target interaction in the free field, it was an enhancement of relatively small values of velocity and dynamic pressure in an absolute sense. Hence, the effect of the 20 percent blockage on target loading from the rapidly-decaying shocks studied here was unimportant, except for shock reflections from the shock tube wall early in the drag phase.

TABLE OF CONTENTS

LIST OF FIGURES

LIST OF FIGURES (Continued)

I. INTRODUCTION

This study examines the effect of blockage on target loading from non-decaying (step) versus rapidly-decaying blast waves. A previous study[1,2] conducted by the Ballistic Research Laboratory (BRL) quantified the effect of shock tube blockage on the net axial loading of a simple target struck by a step shock wave. For that study, the two-dimensional (2-D) cylindrical version of the HULL[3,4] hydrocode was used to simulate a step shock striking a non-responding cylindrical target having its axis coincident with the axis of a cylindrical shock tube. Shocks with overpressures of 34.5 kPa (5.0 psi), 68.9 kPa (10.0 psi), and 137.9 kPa (20.0 psi) were simulated.

That study showed that drag-phase* loading on the target is significantly modified by blockage of the test section by the target. Blockages as small as 10 percent of the cross-sectional area of the shock tube altered loading so that target response was changed significantly. A formula for the proportional increase in dynamic pressure in the constricted region as a function of the blockage ratio was derived. (The constricted region is the region between the target cylinder and the shock tube wall. This region is shown in Figure 1.) This formula, along with a drag coefficient relation, was used in a vehicle overturning code to predict the change (caused by blockage) in the minimum incident shock overpressure required to overturn three representative tactical vehicles. There was some question as to the validity of applying predictions based on non-decaying shock wave results to the more realistic decaying waves modeled in large blast simulators.

---

[1] *N. H. Ethridge, R. E. Lottero, J. D. Wortman, and B. P. Bertrand, "Flow Blockage and its Effect on Minimum Incident Overpressures for Overturning Vehicles in a Large Blast Simulator," Proceedings of the Seventh International Symposium on Military Applications of Blast Simulation, Vol. II, Medicine Hat, Alberta, Canada, 13-17 July 1981.*

[2] *N. H. Ethridge, R. E. Lottero, J. D. Wortman, and B. P. Bertrand, "HULL Hydrocode Computations of Flow Blockage and Its Relation to Overturning of Vehicles in a Large Blast Simulator," (to be published as a BRL Report), US Army Ballistic Research Laboratory, Aberdeen Proving Ground, MD.*

[3] *M. A. Fry, R. E. Durrett, G. P. Ganong, D. A. Matuska, M. D. Stucker, B. S. Chambers, C. E. Needham, and C. D. Westmoreland, "The HULL Hydrodynamics Computer Code," AFWL-TR-76-183, US Air Force Weapons Laboratory, Kirtland Air Force Base, NM, September 1976. (AD #B14070L)*

[4] *J. A. Hasdal, B. S. Chambers, and R. W. Clemens, "Support to BRL: HULL Code Implementation on a CDC 7600," SAI-80-701-AQ, Science Applications, Inc., McLean, VA, August 1979.*

*There are two distinct loading phases: A "diffraction" phase dominated by the initial shock interaction and subsequent interactions of relieving rarefaction waves, and a "drag" phase dominated by drag on the target due to the flow behind the incident shock.

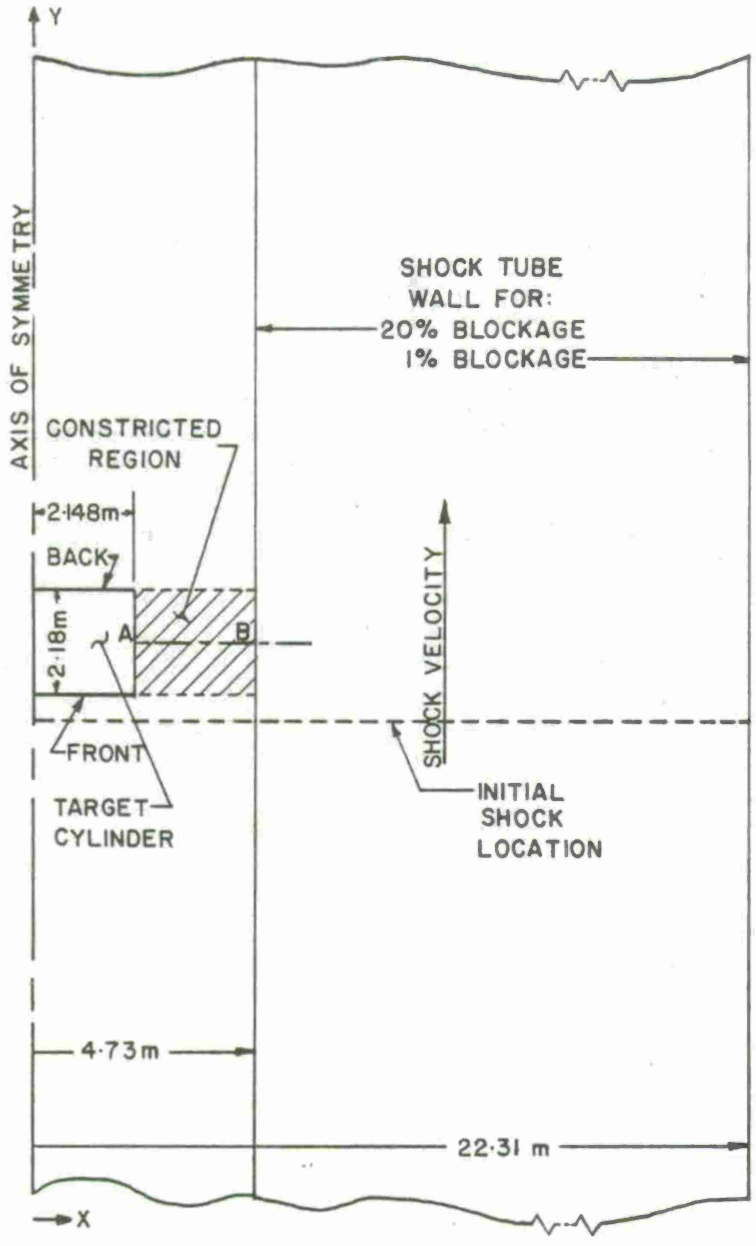

Figure 1. Computational flow fields for 1 and 20 percent blockage.

Hence, a corresponding series of computations for rapidly-decaying shocks having peak overpressures equal to the step shock overpressures was performed. In that way, the two extremes of shock loading encounters could be documented.

Hydrodynamic flow-field variables from the LAMB[5] subroutine coding (curve fits for estimating free-field air blast based on a standard 1 KT* nuclear burst[6]) was used, after modification, to numerically simulate the decaying shock waves. HULL calculations were made for decaying shocks with peak overpressures (corresponding to the step shocks) of 34.5 kPa, 68.9 kPa, and 137.9 kPa. (From this point forward, any reference to, for example, a 34.5 kPa shock refers to a decaying shock with that peak incident overpressure unless specifically stated otherwise.)

The program modifications to HULL are discussed in Section II. The computations are discussed in Section III. Results are presented in Section IV and some conclusions given in Section V.

II. THE COMPUTER CODE

The HULL hydrodynamic computer code used for this project is an airblast version received at the BRL from the Air Force Weapons Laboratory (AFWL) in September 1978. It was modified to run on the BRL CDC 7600 by BRL and AFWL personnel, and by personnel from Science Applications, Inc. (SAI), under contract to the BRL. Other changes were also made by SAI and BRL personnel. This collection of coding is actually a closely-related set of codes, including a grid generator (KEEL), the hydrocode itself (HULL), a plotting code (PULL), and ancillary programs and subroutines.

The program of principal interest, HULL, solves the inviscid Euler equations by an explicit time-step scheme "in the spirit of Lax-Wendroff." The HULL program runs are preceded by a KEEL run which generates the computational grid and initial flow-field conditions. The results can be examined through PULL runs which plot and print results stored by HULL. Each of these programs is a collection of subroutines and coding from which appropriate code is selected by a preprocessor.

Changes were inserted in both the KEEL and HULL codes to simulate planar decaying shocks. All the shock waves simulated for this study had a plane front. The value of pressure and other hydrodynamic variables for the

---

[5] *C. E. Needham and L. A. Wittwer, "The Air Force Weapons Laboratory Low Altitude Multiple Burst (LAMB) Model," AFWL-DYT-75-2 (unpublished).*

[6] *C. E. Needham, M. L. Havens, and C. S. Knauth, "Nuclear Blast Standard (1KT)," AFWL-TR-73-55 (Rev.), US Air Force Weapons Laboratory, Kirtland Air Force Base, NM, April 1975. (AD #A014850)*

*kilo-ton TNT, blast equivalent.

decaying shock waves decreased as the distance behind the shock front increased. (The step shocks in the previous study had constant hydrodynamic values behind the front.)

A preliminary program, independent from HULL except that it used the same LAMB subroutines, was used to determine the time at which the shock front reached the desired overpressure. It was also used to compute the distance to the shock front from the burst point (which is outside of the computational grid for HULL) and the approximate decay rate behind the shock. Runs of about 120 ms (over 20 crossing times* of the target) were desired; these were typical run times for the step shock cases. For a 100 KT ground burst, for example, the overpressure at a radius of 1.48873 km (the distance from the burst point to the position where the incident shock overpressure reached 68.9 kPa) decayed by 19 percent to 55.8 kPa in 120 ms. Similarly, for ground bursts of 10 KT, 1 KT, and 0.1 KT the decay during that time for a 68.9 kPa incident shock was 37, 64, and 96 percent, respectively. The 0.1 KT yield was chosen because it represented an extreme case of nearly complete overpressure decay within the simulated time. This yield was also used for the 34.5 kPa and 137.9 kPa shocks.

The planar decaying shock waves were produced by transforming the spherical shock wave from the LAMB coding into a planar wave in HULL by mapping sea-level flow-field variables from LAMB into HULL and using the velocity magnitude from LAMB for the axial component of velocity. The effective rotation of the velocity vector from a spherical coordinate system to a direction parallel to the axis of symmetry in a cylindrical coordinate system had the following effect. The transformation of the velocity vector from LAMB to the velocity vector in the shock tube is exact on the axis of the shock tube. (The axis is assumed to point toward the burst point.) At radial positions away from the axis, the LAMB velocity vector has two additional velocity components (if viewed in a three-dimensional Cartesian coordinate system). The "elimination" of these velocity components by this rotation of the vector caused increasingly larger "error" as the radial position in the shock tube increased. For the 1 percent blockage case, this error, at the entrance of the shock tube, ranged from 0 at the axis of symmetry to 3.4 percent at the outer-radial boundary. Once the computation was begun, the flow was constrained by the outer-radial boundary of the shock tube. This produced a shock wave which was different from that for a point-source blast wave because there was no further radial divergence in the shock tube.

Because the LAMB values for flow-field variables were computed from fitted curves, they are not necessarily self-consistent. Further, the velocity transformation used here produced some inconsistencies because the momentum equations in cylindrical coordinates do not contain the same radial divergence terms as in spherical coordinates. Once the HULL computation was begun, the input flow-field variables were used in the

*A crossing time is defined as the time required for the incident shock to travel the axial length of the target. The crossing time for the 68.9 kPa shock is 5.1 ms.

difference equations for cylindrical coordinates (with a no-outflow condition imposed at the outer-radial boundary) to compute mass, momentum, and energy transfer. This caused a set of perturbing waves to occur, further modifying the blast wave which was initially mapped into the computational grid.

The resulting shock wave in HULL and the comparable shock wave from LAMB are shown in Figures 2 and 3. Figure 2 shows the distribution of side-on overpressure and dynamic pressure as functions of radial distance for the spherical blast wave from LAMB and axial distance for the modified, planar blast wave in an empty shock tube. For convenience, the location of the front face of the target (if it were in the grid) is redefined as 0.0. The profile shown in Figure 2 is taken at 18.73 ms after the incident shock passed the position where the front face would be. The absence of radial divergence in the blast wave in the simulated shock tube is evident in both the side-on overpressure and the dynamic pressure curves, with the LAMB values less for both. Figure 3 shows similar curves at 43.73 ms. Here, the differences are even greater. Note the distinctly earlier arrival time for the stronger planar shock wave and a distinct compression wave between -20.0 and -5.0 m. This compression wave is probably due to the mismatched initial flow conditions mentioned earlier.

This modification of the blast wave is not of direct concern for this problem. The intent was only to simulate a rapidly-decaying blast wave. However, this discussion does serve to point out the need for caution in attempting to use a simplified technique such as this if a specific yield is to be simulated.

The LAMB coding associated with HULL was recently used to simulate a decaying shock for a three dimensional (3-D) problem,[7] with the radial divergence included. The original plan was to simply transfer some of this coding into the 2-D portions. However, the 2-D coding for HULL already contained part of the needed programming (with a slightly different approach) so it was used, because fewer changes were needed.

The grid generation program, KEEL, was modified to initiate the computation with the computational flow field in the cylindrical shock tube partly filled by the decaying, planar shock wave. The HULL program was changed to allow continuous input of this decaying wave at the bottom boundary of the grid. (In HULL terminology the radial coordinate, X, increases from left to right and the axial coordinate, Y, increases from bottom to top.)

---

[7] *J. D. Wortman, "Blast Computations over a Hemicylindrical Aircraft Shelter," ARBRL-MR-03115, US Army Armament Research and Development Command, Ballistic Research Laboratory, Aberdeen Proving Ground, MD, July 1981. (AD #B058960L)*

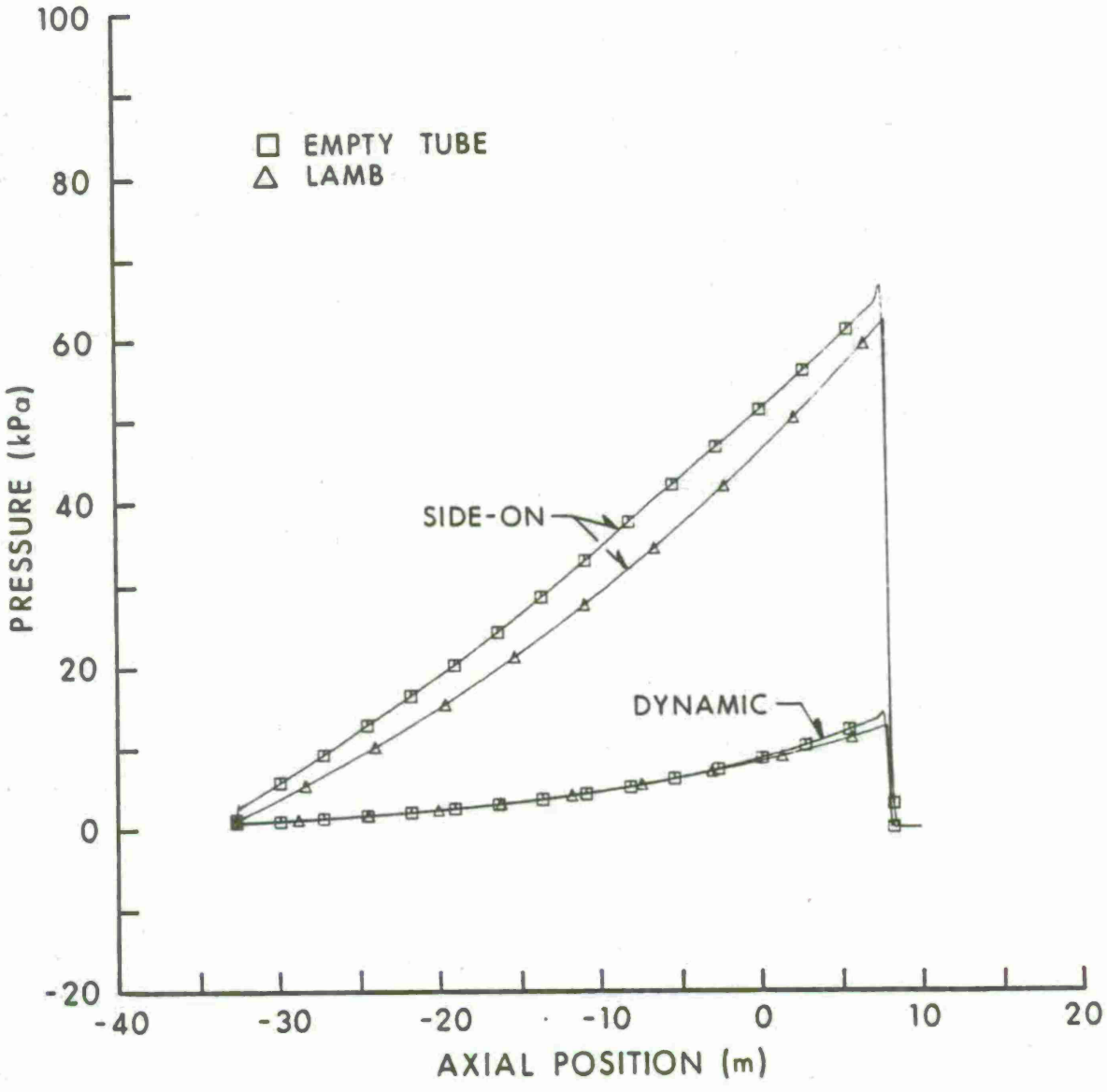

Figure 2. Side-on overpressure and dynamic pressure versus distance for the LAMB blast wave and the planar HULL blast wave, 18.73 ms after the incident shock passes the front face location.

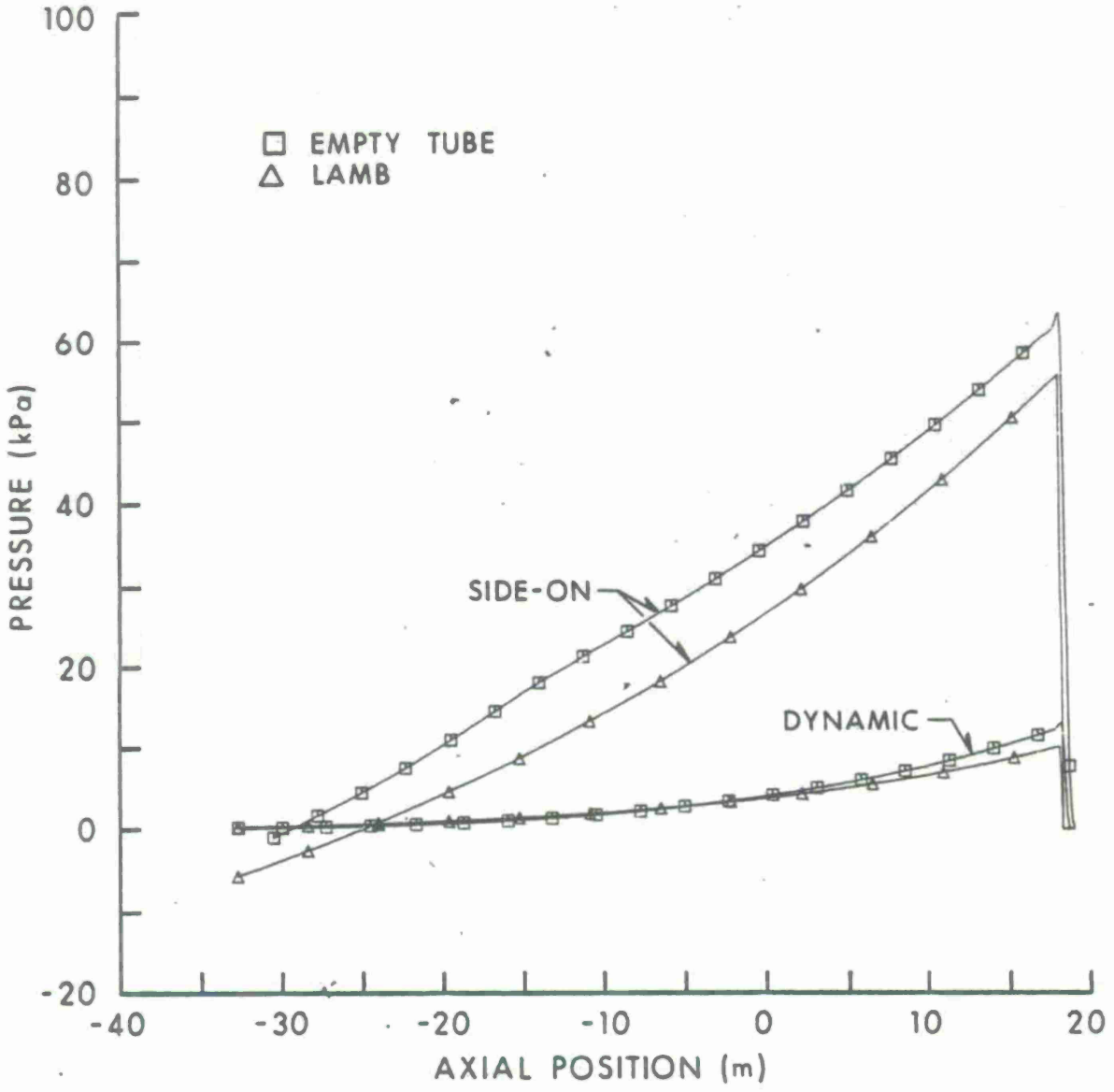

Figure 3. Side-on overpressure and dynamic pressure versus distance for the LAMB blast wave and the planar HULL blast wave, 43.73 ms after the incident shock passes the front face location.

III. COMPUTATIONS

The first set of hydrocode computations for the decaying shocks was made for a nominal 20 percent blockage for all three shock strengths. The grid for the 20 percent blockage was the same as that for the step shock study,[1,2] except the simulated shock tube was made a little longer. The computational grid extended in the axial direction 32.7 m upstream from the front face of the 2.18 m long target cylinder, and 19.62 m downstream from the back face of the target cylinder. This total axial distance of 54.5 m was divided into 500 equal computational flow field cells (ΔY = 10.9 cm), including 20 cells for the target length. The computational grid extended radially from the axis of symmetry (at X = 0.0) to X = 472.56 cm, with 44 equal cell divisions (ΔX = 10.74 cm). The target extended radially from X = 0.0 to X = 214.8 (20 ΔX divisions). The radius of the target was chosen so that the front face area would match the presented cross-sectional area of a communications shelter on a 2½ ton truck parked with its sides parallel to the incident shock front. (The 20 percent blockage approximates the blockage caused by the truck with shelter in the large blast simulator at the Centre d'Etudes de Gramat, Gramat, France.[8,9]) The axial length of the target was equal to the distance across the shelter in the direction of travel of the shock.

Runs were also made for an empty (i.e., unobstructed) shock tube for each of the three decaying shocks to provide reference flow-field data. In these cases there was no target and only 4 cells in the X direction. Otherwise, these runs were like the blockage runs.

In addition, one run with a 68.9 kPa shock was made to simulate a target in a free field. A large-radius shock tube was simulated by using 100 equal divisions in the X direction with ΔX = 10.74 cm, followed by 38 divisions with geometrically increasing widths (a cell-to-cell ratio of 1.05) out to X = 2230.797 cm. This produced a blockage of less than 1 percent. Because there was no return of a wave from the reflective outer-radial boundary of the shock tube to the target during the run, and only the axial force on the target was of interest, this was effectively a free-field (no blockage) computation. This was still not like a point-source shock wave in the free field; the shock wave was a plane wave.

In all the HULL computations, the shock front was initially located at 54.5 cm (5 computational cells) upstream from the front face of the target. For the step shocks, all the cells 6 or more cells upstream from the front

---

[8] *J. R. Crosnier and J. B. Monzac, "Large Diameter High Performance Blast Simulator," Proceedings of the Fifth International Symposium on Military Applications of Blast Simulation, Stockholm, Sweden, May 23-26, 1977.*

[9] *J. R. Crosnier, S. Gratias, J. B. Monzac, and H. Richard, "Concepts and Design for a Large Diameter High Performance Blast Simulator," Proceedings of the Fourth International Symposium on Military Applications of Blast Simulations, Southend-on-Sea, England, September 9-12, 1974.*

face of the target were filled with shocked air at the uniform state of the gas behind the shock. For the decaying shocks, subcell, mass-weighted, average values from the LAMB computation were put in each of these cells.*

During the HULL runs, the decaying shock computed by LAMB was fed in through the bottom boundary of the grid as a function of time. The top boundary was transmissive. Both of these boundaries were far enough from the target that no false reflections from them reached the vicinity of the target during the runs. An axis of symmetry existed at X = 0.0; the outer-radial boundary was reflective.

Various time references were used for different parts of the study. The KEEL runs were initiated with times set between 100 and 400 ms; these times corresponded to the times at which the shock front in LAMB decayed to the desired level. These times were transferred to LAMB to produce consistent initial flow-field conditions for HULL. When the HULL runs were initiated, the time was reset to 5 ms for HULL so that HULL would produce restart dumps containing all of the flow-field data at intervals matching those for the step shock runs. The correct time shift to use imput values from LAMB was introduced by temporary coding in HULL. For the remainder of this report, for convenience and consistency, time is redefined to a reference value of t = 0.0 at the theoretical shock arrival at the front face of the target.

IV. COMPARATIVE RESULTS

Figure 4 shows gas velocity (hereafter referred to as "particle velocity") vector plots for the 68.9 kPa step shock run at 3.7, 13.7, and 103.7 ms. Figure 5 shows corresponding particle velocity vector plots for the decaying shock with 68.9 kPa overpressure. The times are referenced to zero for shock arrival at the front face. The HULL plotting procedure plotted the velocity vectors from about every fourth cell in both directions.

Figures 4a and 5a show velocity vectors after about 0.7 of a crossing time. At this time, the vector plots are nearly the same. Figures 4b and 5b show velocity vectors after about 2.7 crossing times. At this time the target (the clear area in the velocity vector plots) has been completely enveloped by the shock. The two plots are now a little different, primarily due to a difference in scaling of the velocity vectors. The greatest particle velocity in the flow field at this time for the step shock is 210 m/s. Hence, the scaling is 250 m/s per inch (of the original-scale plotting surface). The maximum velocity for the decaying shock is 191 m/s and the scaling is 200 m/s per inch. Figures 4c and 5c show the velocity vectors after 20 crossing times. There are now significant differences between the two cases. The maximum velocity for the decaying wave case is 57 m/s while the maximum

*Each cell was subdivided into 9 subcells, and each subcell was filled with shocked air behind the decaying shock front as calculated by LAMB subroutines for sea level at a distance from ground zero corresponding to the subcell center.

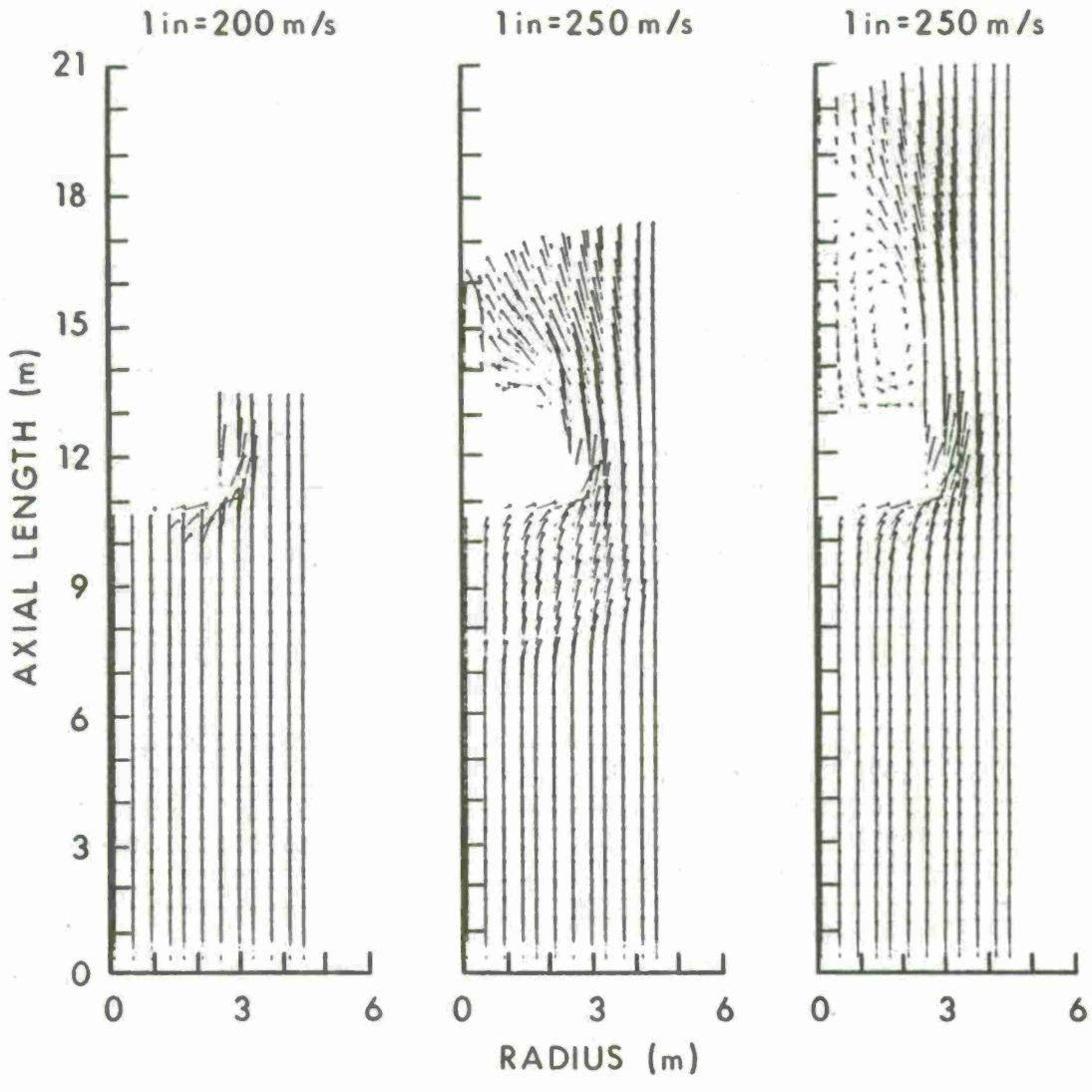

Figure 4. Particle velocity vector plot for a 68.9 kPa step shock with 20 percent blockage at (a) 3.7 ms, (b) 13.7 ms, and (c) 103.7 ms.

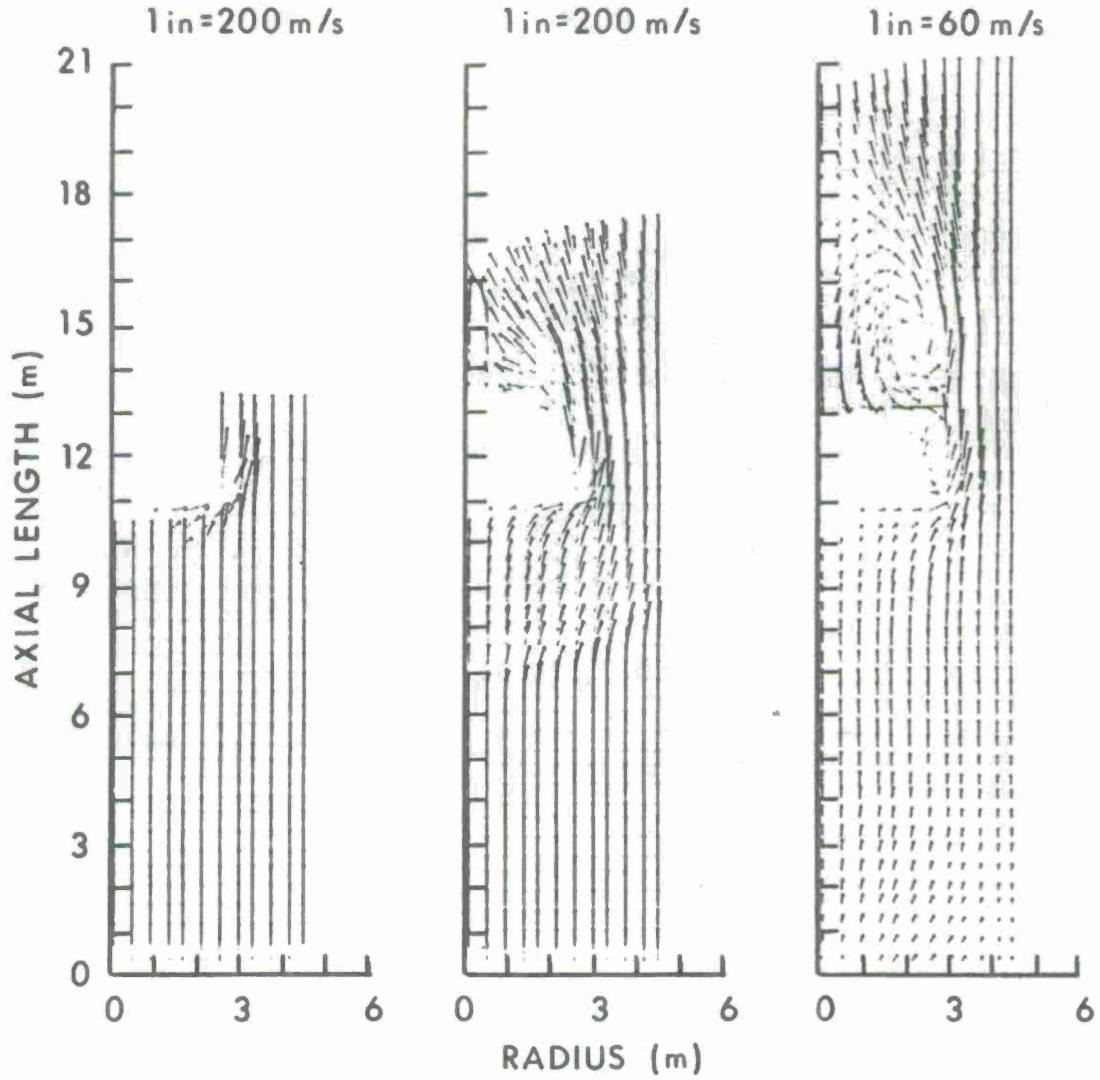

Figure 5. Particle velocity vector plot for a 68.9 kPa decaying shock with 20 percent blockage at (a) 3.7 ms, (b) 13.7 ms, and (c) 103.7 ms.

velocity for the step shock case is 201 m/s. The decaying wave case has a significant vortex on the side of the target and the velocity magnitudes near the back face are greater than those near the front.

Figure 6 shows the force on the front face of the target, the force on the back face, and the net axial force (force on the front minus force on the back) for the 68.9 kPa decaying shock with 20 percent blockage. The force on a face is obtained by integrating the overpressure over the area of that face.

It is instructive to follow the loading process. When the incident shock strikes the front face of the target, the pressure behind the reflected shock builds up quickly to 2.53 times the incident shock overpressure and then decays due to the passage of a strong expansion wave travelling radially (inward) across the face. This expansion wave was initiated at the outer edge of the front face immediately after the reflection of the incident shock. The reflected shock expands radially, weakening continuously. It eventually arrives at the reflective outer-radial boundary of the shock tube and reflects from it. When this reflected wave reaches the front face again, the force there is enhanced, reaching a local maximum. It then reflects from the axis of symmetry, and travels back toward the outer-radial boundary. Reflected waves continue to move back and forth radially for an extended period of time, thus the successive local maxima and minima.

After one crossing time the shock front begins to load the back face. The force on the back face increases as the shock front travels along the back face toward the axis of the shock tube. The force is enhanced by the reflection of the shock front at the axis of the tube, and by the arrival of the first reflected wave from the outer-radial boundary of the shock tube. For the example in Figure 6, the net force approaches zero after 3.4 crossing times and becomes negative 3.2 crossing times later. This initially surprising result is discussed later.

The histories of net axial force on the target for the three shock strengths are plotted in Figures 7, 8, and 9. The three figures are all similar. During the drag phase, the net forces from the step shocks oscillate about positive values, and the net forces from the decaying shocks oscillate about negative values. For each shock strength, the frequencies of the oscillations are approximately the same for the step shock and the decaying shock. This is also true for the amplitudes of the oscillations for the two weaker shocks. For the 137.9 kPa shock, the amplitude of the oscillations for the step shock is damped more rapidly than that for the corresponding decaying shock because of the near choking condition in the constricted region for the step shock.

The net forces for the free-field runs are included in Figure 8. This shows the effects of blockage on the net force. The 20 percent blockage has negligible effect during the diffraction phase ($t < 20$ ms). In fact, it has no effect until the reflected shock travels to the outer-radial boundary of the shock tube and back to the target (about 3 crossing times). The increased net force due to blockage is clearly shown for the step shock. After the net

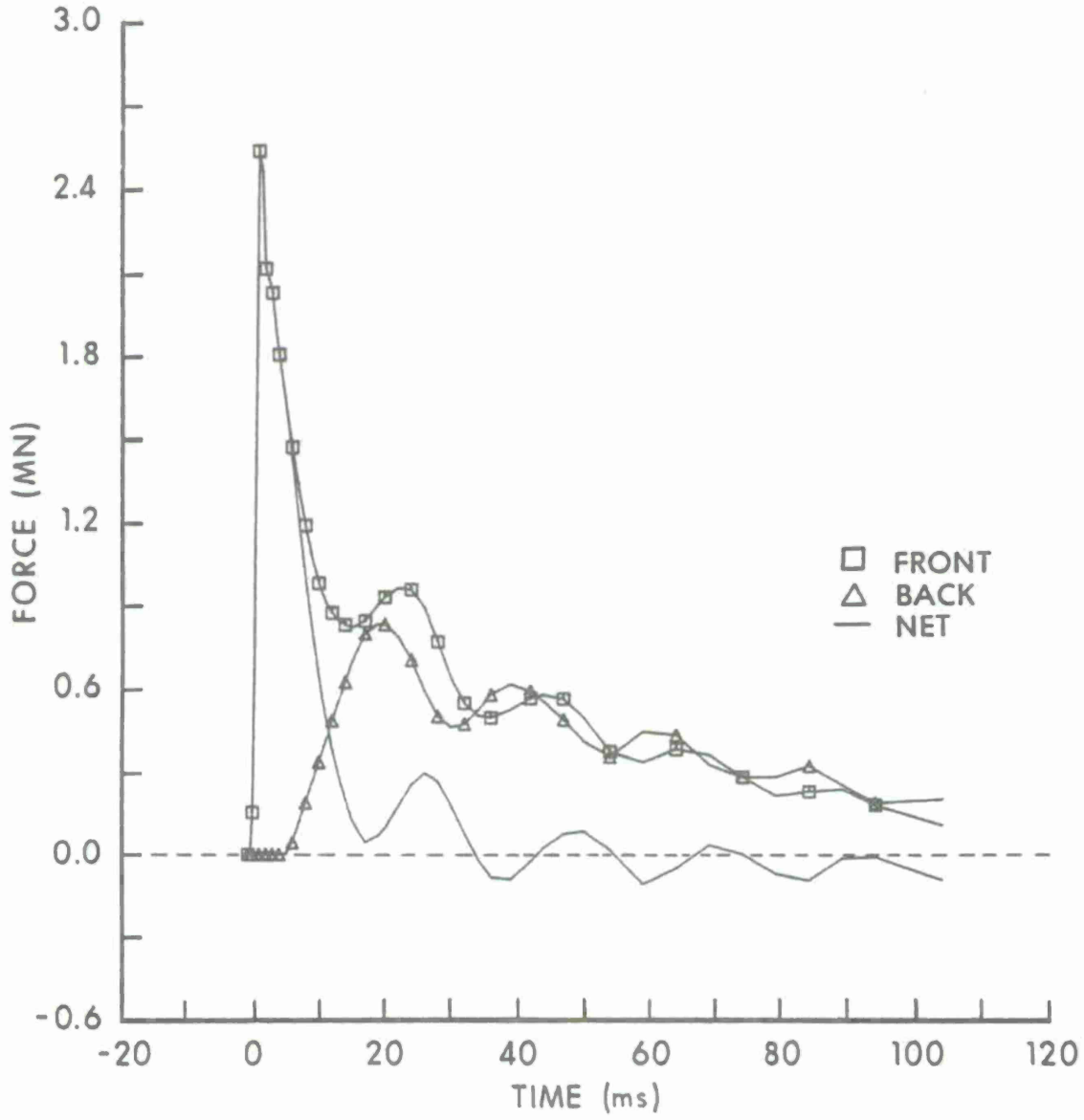

Figure 6. Axial forces on the target cylinder for a 68.9 kPa decaying shock with 20 percent blockage.

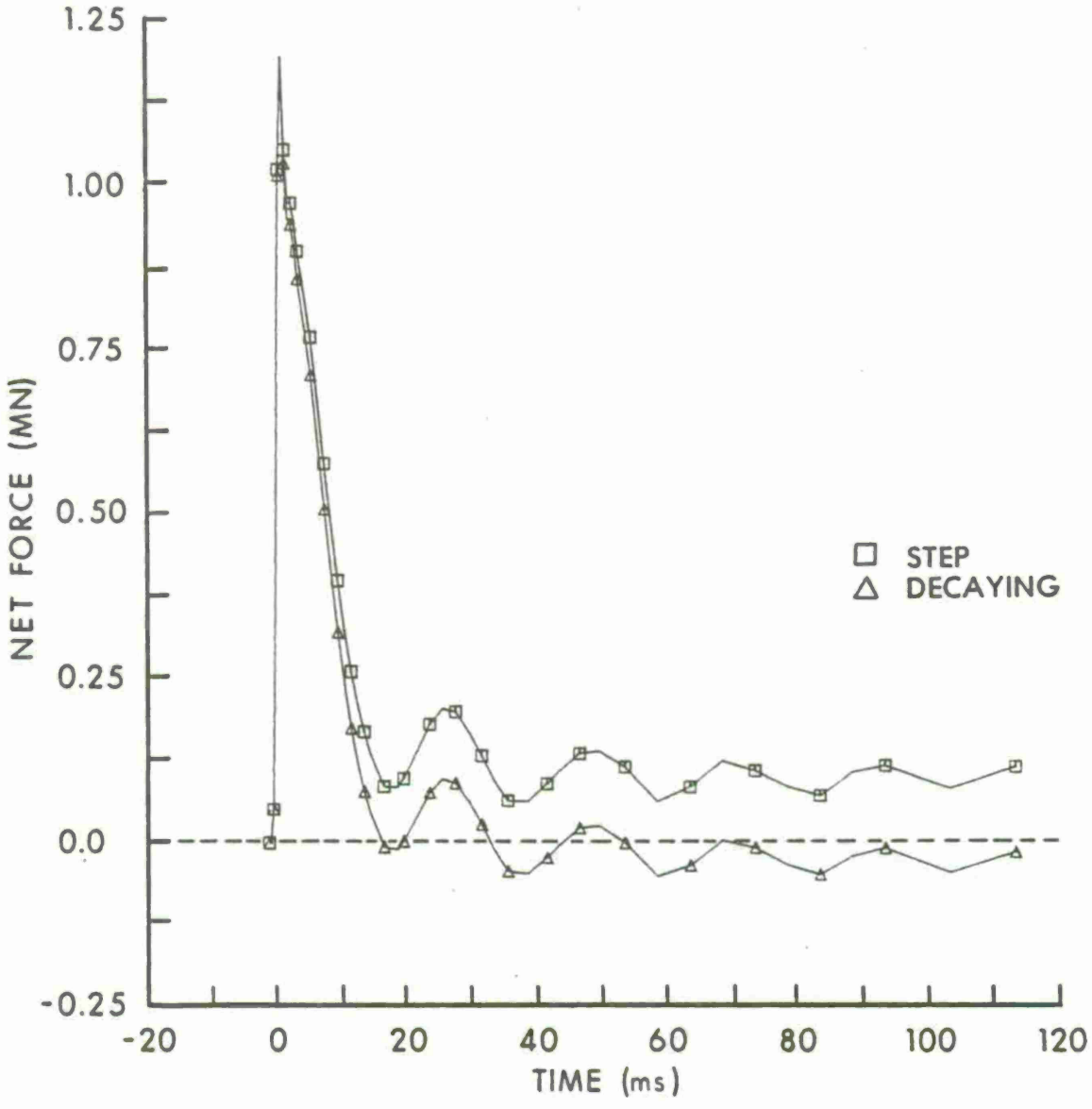

Figure 7. Net axial force on the target cylinder for 34.5 kPa decaying shocks with 20 percent blockage.

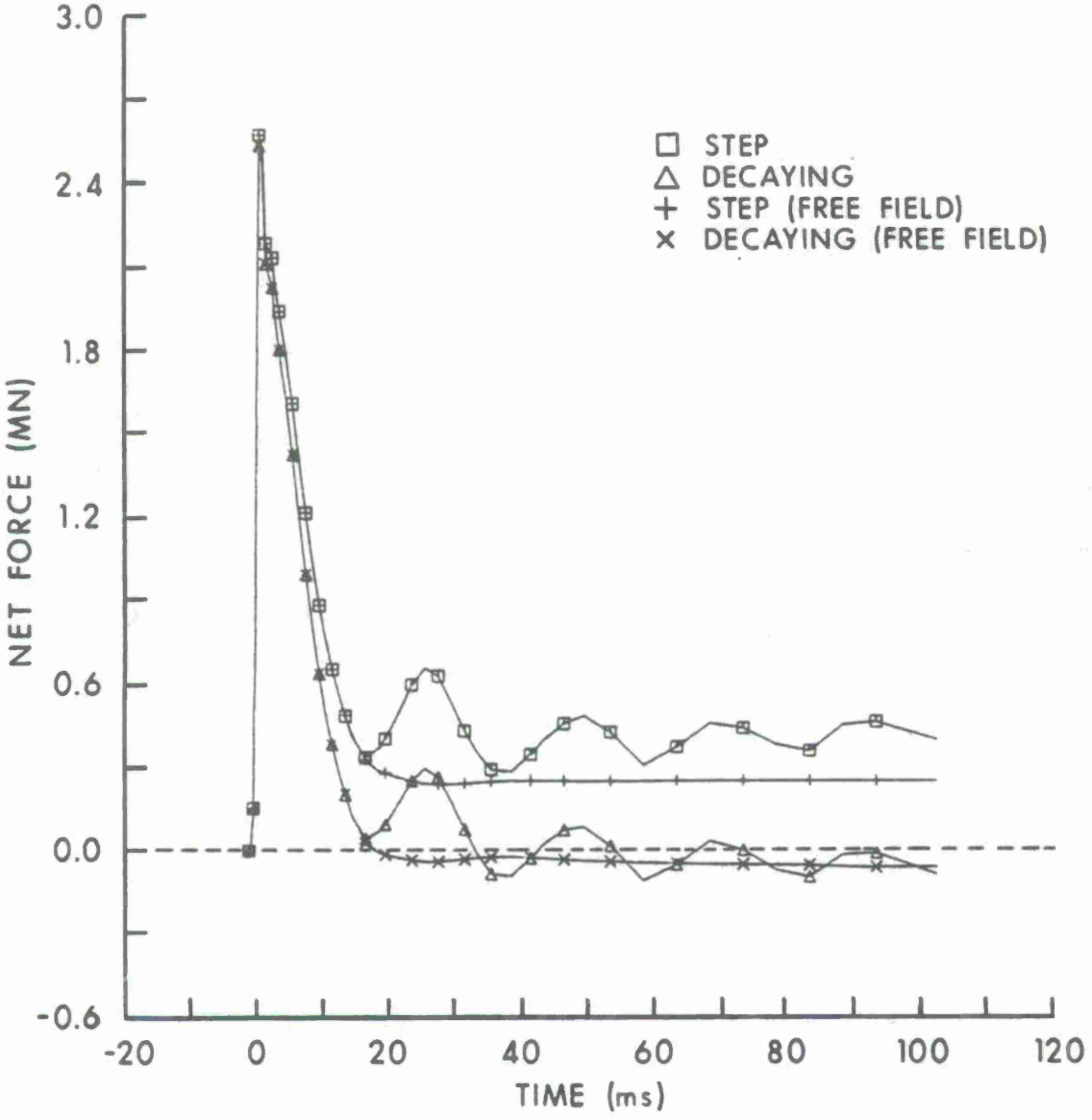

Figure 8. Net axial force on the target cylinder for 68.9 kPa shocks with 20 percent blockage.

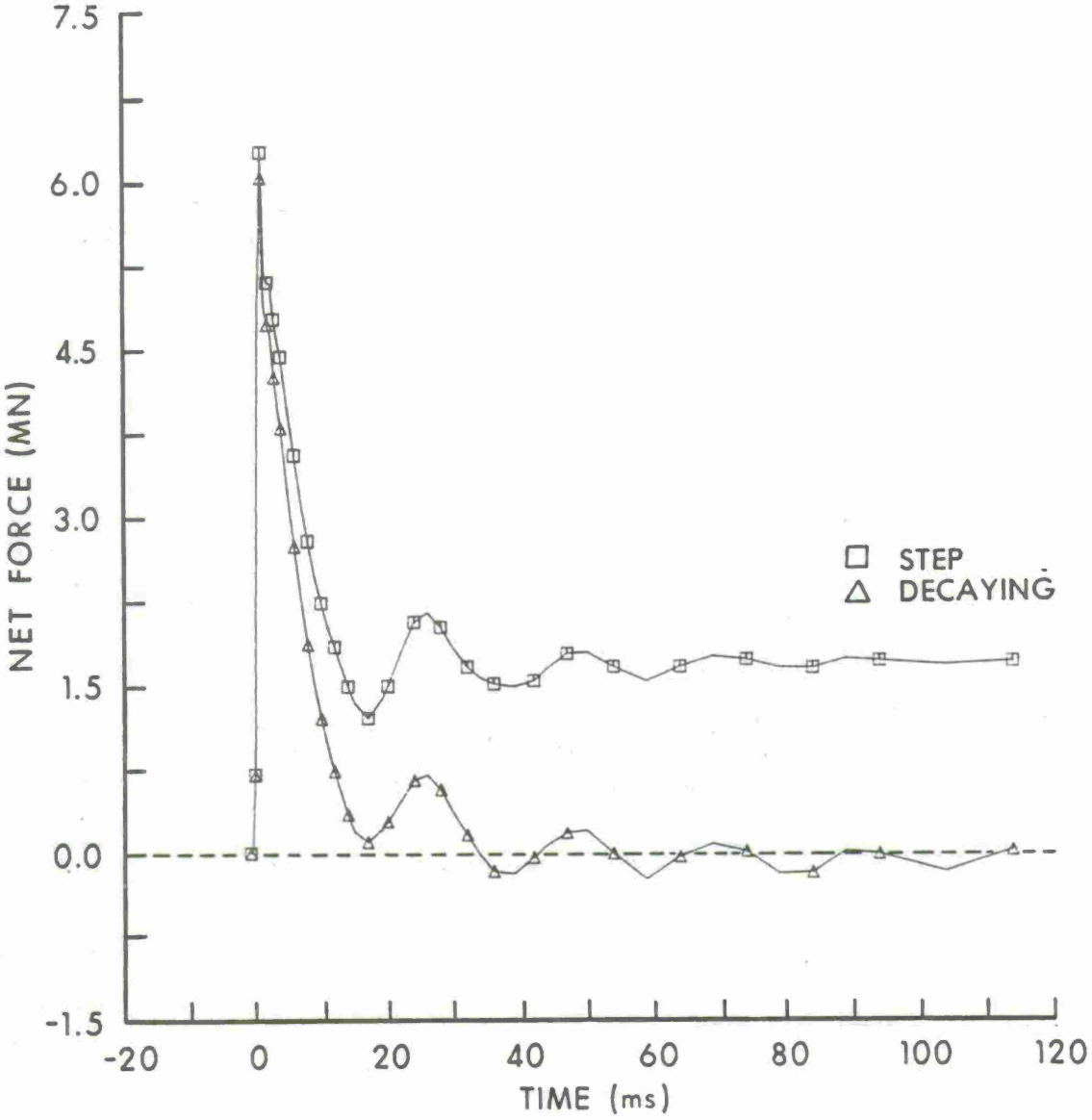

Figure 9. Net axial force on the target cylinder for 137.9 kPa shocks with 20 percent blockage.

force for the decaying shock becomes negative (at about 30 ms) there is very little obvious blockage effect except for oscillation. The net force for the decaying shock in the free field becomes negative much earlier and remains negative for the duration of the run (which did not reach the end of the positive phase of the shock wave).

It was initially surprising that the net axial force for the decaying shocks became negative while the bulk movement of the surrounding gas was still in the positive direction. This negative net force is not due to the blockage, but rather is due primarily to the rapid decay of the simulated blast wave. Once the shock front passes the plane of the back face, this causes a higher side-on overpressure in the plane of the back face of the target than at the front. The spatial distribution of pressure can be seen in Figures 2 and 3. Figure 10 shows the side-on overpressure and the dynamic pressure versus time at the location of the target front face for both the LAMB blast wave and for the empty shock tube computation using the modified planar blast wave. Figure 11 shows the same curves at the location of the back face. After the peak overpressure is reached on the back face, the side-on overpressure in the plane of the back face is greater than that in the plane of the front face of the target. This is at least partially compensated for by the drag force on the target, computed by

$$F_D = C_D(\tfrac{1}{2}\,\rho\,V_a^2), \qquad (1)$$

where C_D is a drag coefficient (≈ 1.2) and $\frac{1}{2}\,\rho\,V_a^2$ is the dynamic pressure (in the axial direction) at the plane of the front face. Here, ρ is the density and V_a is the particle axial velocity. It is interesting to note that there is relatively little difference in the dynamic pressure for the two blast waves.

The net force on the target for these decaying shocks in the free field (see Figure 8) becomes negative somewhat sooner than expected. HULL may be computing a slightly higher pressure on the back face than it should. There should be at least a modestly-sized annular region of relatively low pressure on the back face of the target due to the generation of a toroidal vortex. HULL has been demonstrated to significantly underestimate the strength (hence overestimate the pressure) of a strong cylindrical vortex for a 2-D Cartesian computation with similar resolution.[2] It may be making a similar, but much smaller, error in this case, thereby causing the net force to become negative sooner than expected. For the one unblocked decaying shock case (shown in Figure 8), the net force becomes negative after about 4 crossing times and stays negative for the remainder of the computation.

Figures 12, 13, and 14 show the net axial total impulse* on the cylindrical target for the various cases. The results are similar for all three shock strengths. The net impulse increases rapidly from the time the

*Total impulse is computed by successively summing the product: (average force due to overpressure on a target face during a time interval) times (the time interval).

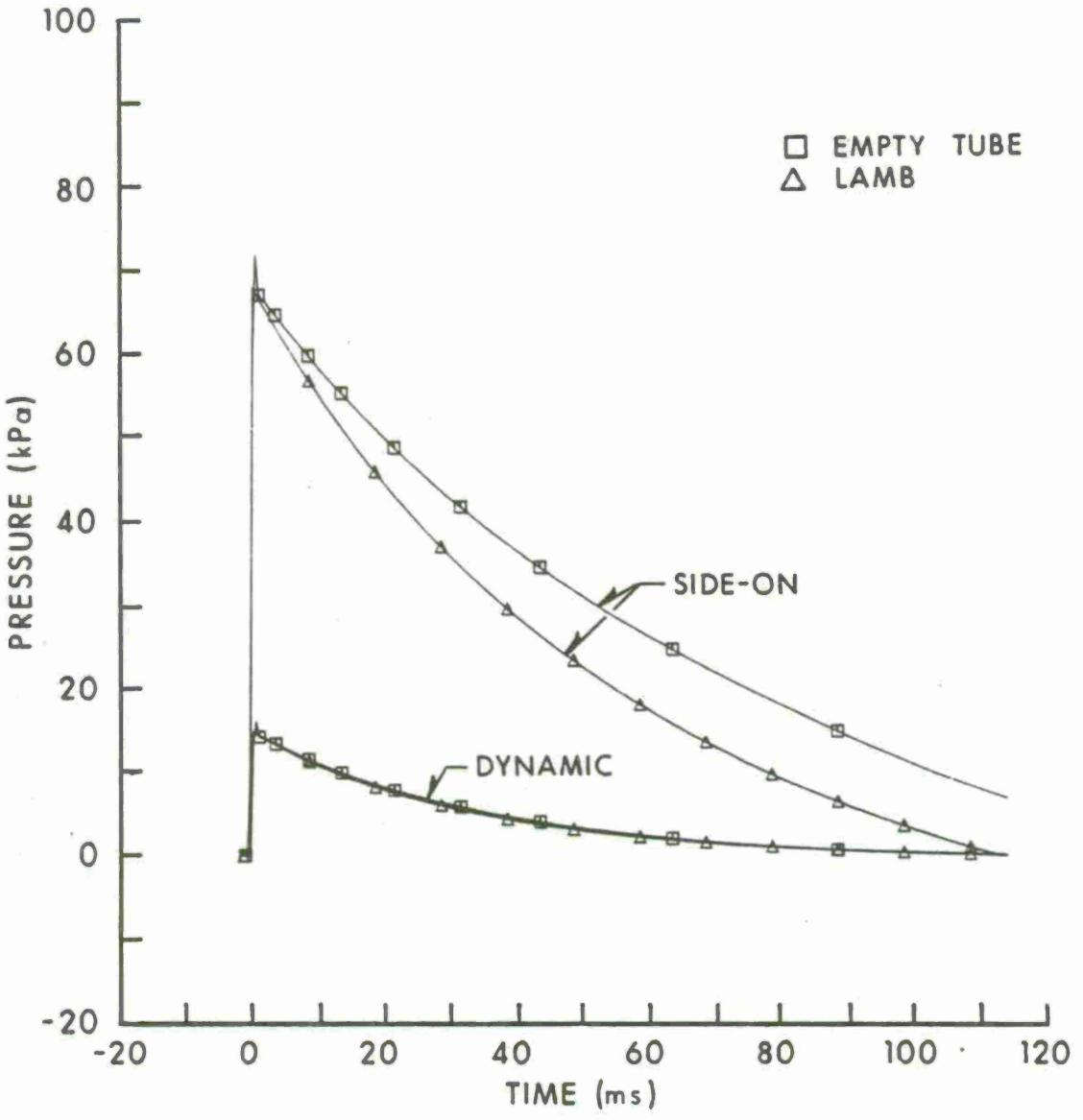

Figure 10. Side-on overpressure and dynamic pressure versus time for the LAMB blast wave and the planar HULL blast wave at the location of the front face.

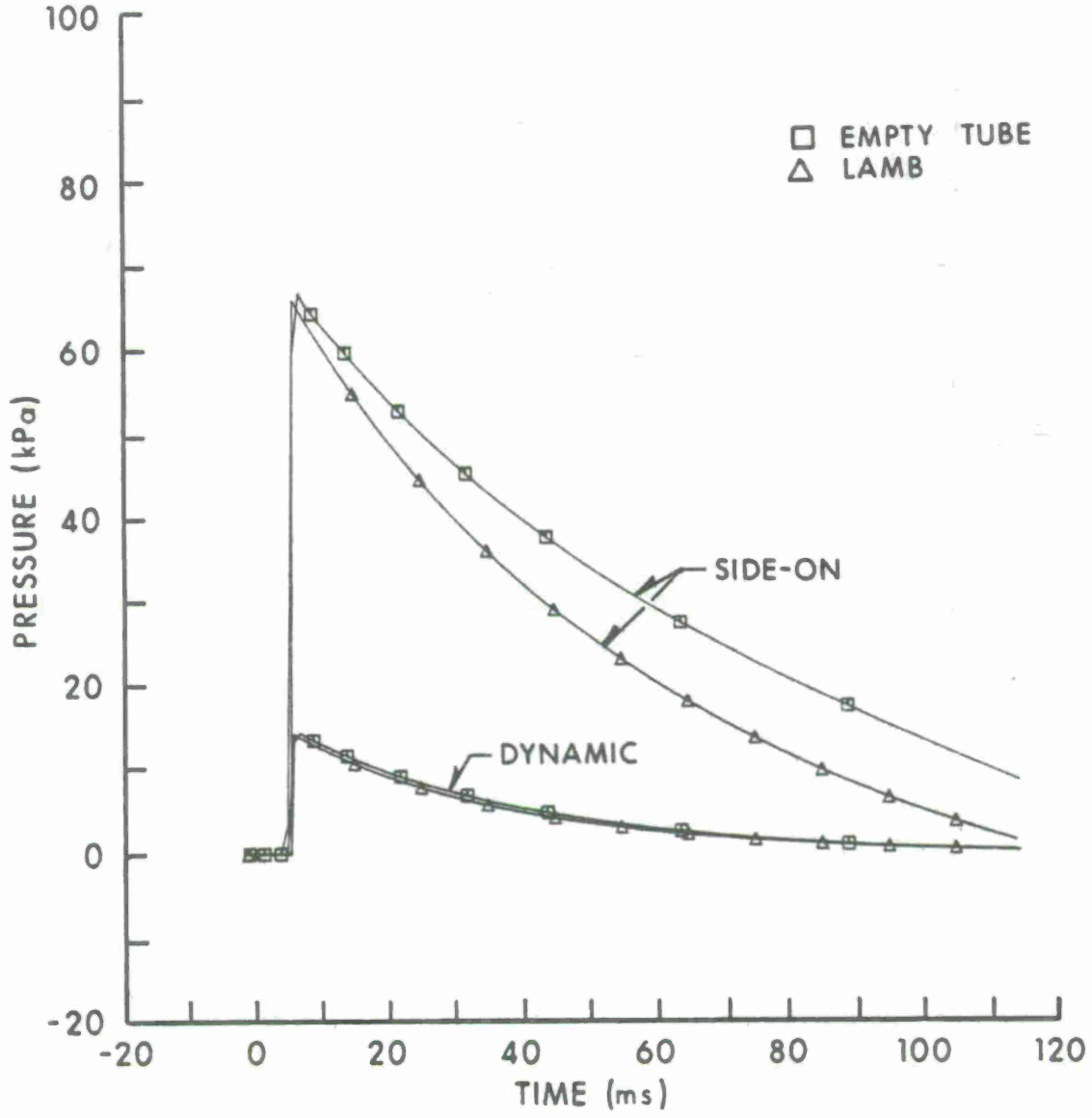

Figure 11. Side-on overpressure and dynamic pressure versus time for the LAMB blast wave and the planar HULL blast wave at the location of the back face.

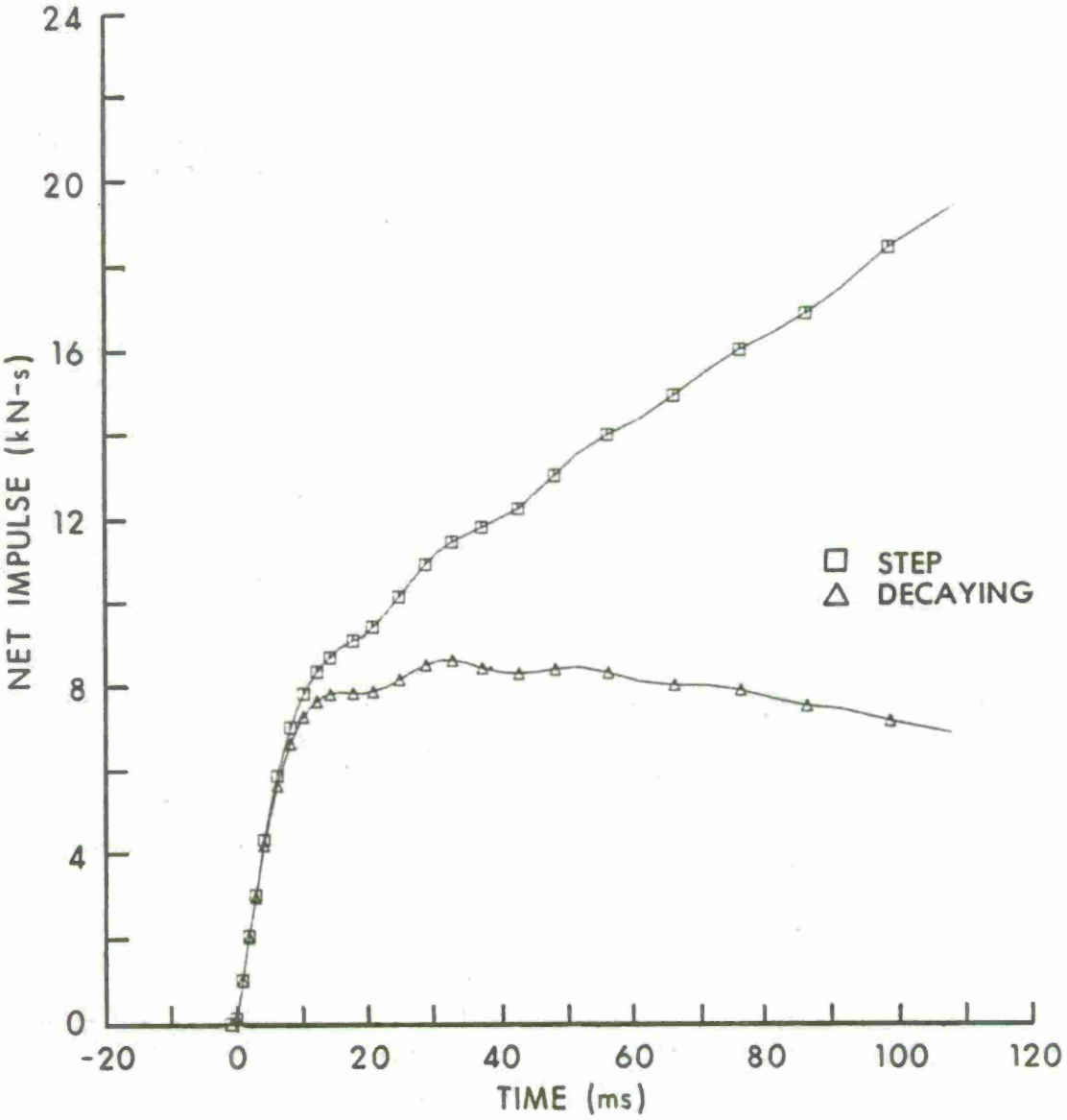

Figure 12. Net axial impulse on the target cylinder for 34.5 kPa shocks with 20 percent blockage.

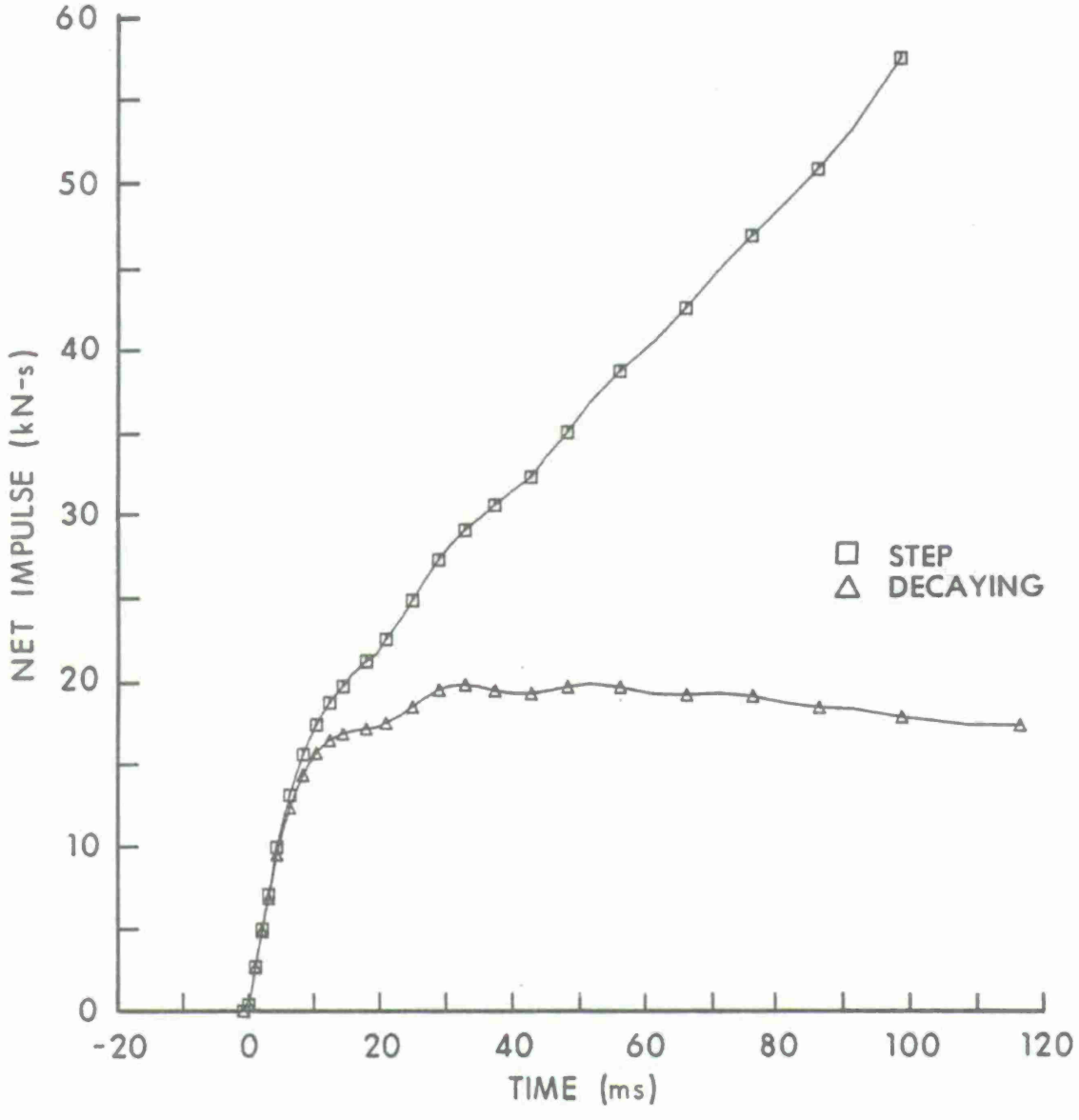

Figure 13. Net axial impulse on the target cylinder for 68.9 kPa shocks with 20 percent blockage.

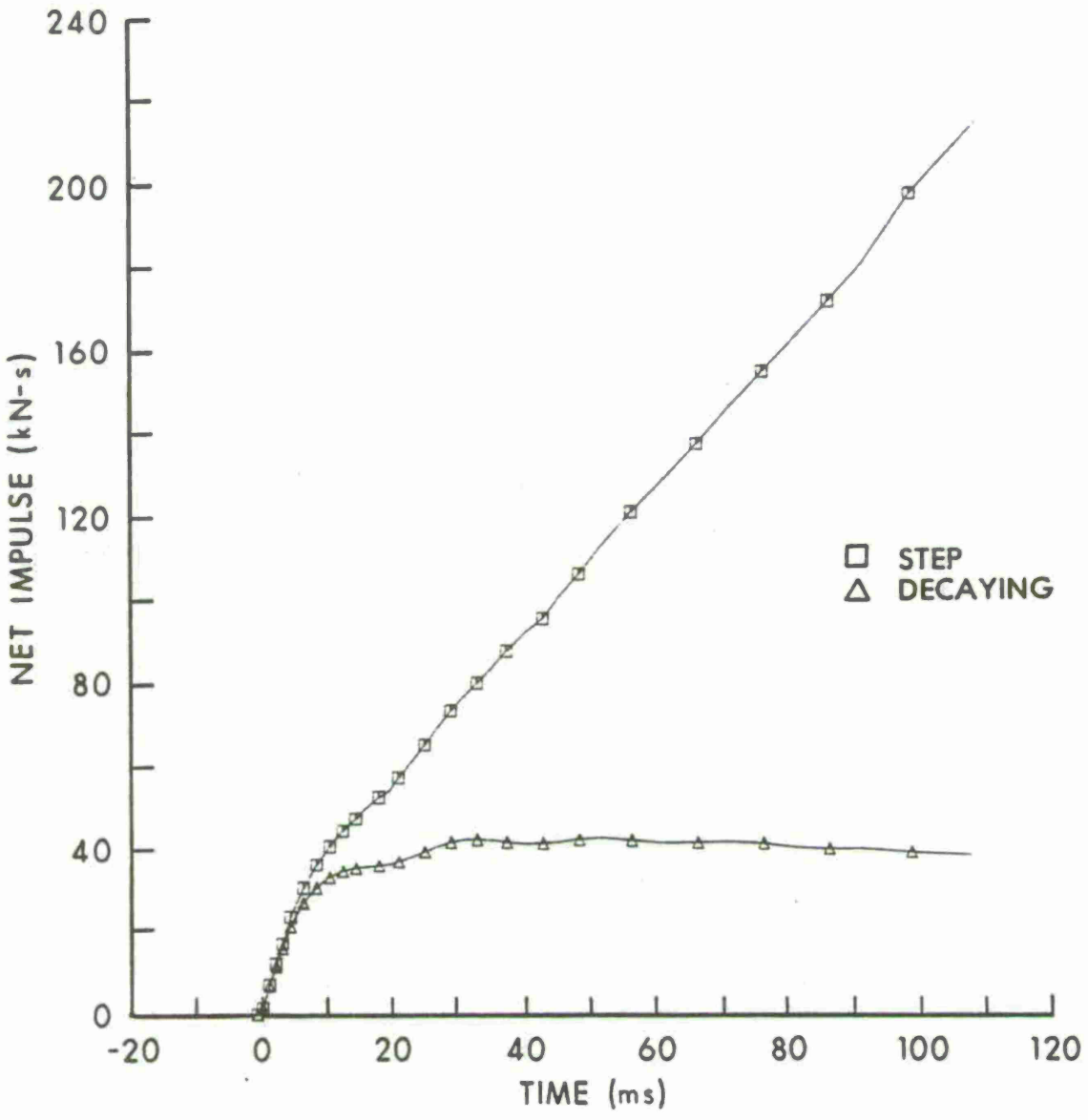

Figure 14. Net axial impulse on the target cylinder for 137.9 kPa shocks with 20 percent blockage.

incident shock strikes the target until the blast wave envelops the target. The net impulse for the step shocks then increases at a steady rate, consistent with the positive net force. The net impulse for the decaying shocks reaches a maximum and then slowly decreases; this is consistent with having negative net force on the target.

Figures 15, 16, and 17 show the average magnitude of the particle velocities in the constricted region in a line of cells from the center of the side surface of the target to the outer-radial boundary. (See line AB, Figure 1.) The particle velocity initially increases rapidly for both types of shock. The velocity for the step shocks then increases slowly to a plateau value. For the decaying shocks, the increase after the initial jump is smaller than that for the step shock (with no further increase for the 137.9 kPa decaying shock); the average velocity magnitude then decreases steadily from a local maximum which occurs shortly after the initial peak.

Figures 18, 19, and 20 show the average dynamic pressure, $\frac{1}{2} \rho V^2$, (V is the particle velocity magnitude) in the constricted region averaged across the same row of cells as the particle velocity. In addition to the dynamic pressures for the 20 percent blockage runs, these figures include the dynamic pressure for the decaying shock in an empty tube. This reaches a peak value and decreases smoothly toward zero. The corresponding dynamic pressure for a step shock in an empty tube is a step function, which jumps from zero to a constant value.

Figures 21, 22, and 23 show the effect of blockage on the normalized average dynamic pressure in the constricted region for the step shocks and the corresponding decaying shocks. The average dynamic pressure for the step shock is normalized by dividing by the dynamic pressure (3.995 kPa, 15.27 kPa, and 56.11 kPa for the 34.5 kPa, 68.9 kPa, and 137.9 kPa shocks, respectively) behind the incident shock prior to its interaction with the target. The dynamic pressure of the decaying wave for computations where blockage is simulated is normalized by dividing by the corresponding dynamic pressure at that time from the empty-tube computation. The dynamic pressures for the decaying shocks become smaller as time progresses, ultimately making the normalized values meaningless. However, the blockage effect on dynamic pressure is greater in a relative sense for the decaying shocks than for the step shocks.

The relation developed in References 1 and 2 to predict the increase in dynamic pressure due to blockage is

$$Q_B/Q_o = e^{(2.64\ R^{1.038})}, \qquad (2)$$

where: Q_B = average dynamic pressure with blockage present,

Q_o = free-field dynamic pressure with no blockage,

R = blockage ratio, the cross-sectional area of the target divided by the cross-sectional area of the shock tube test section.

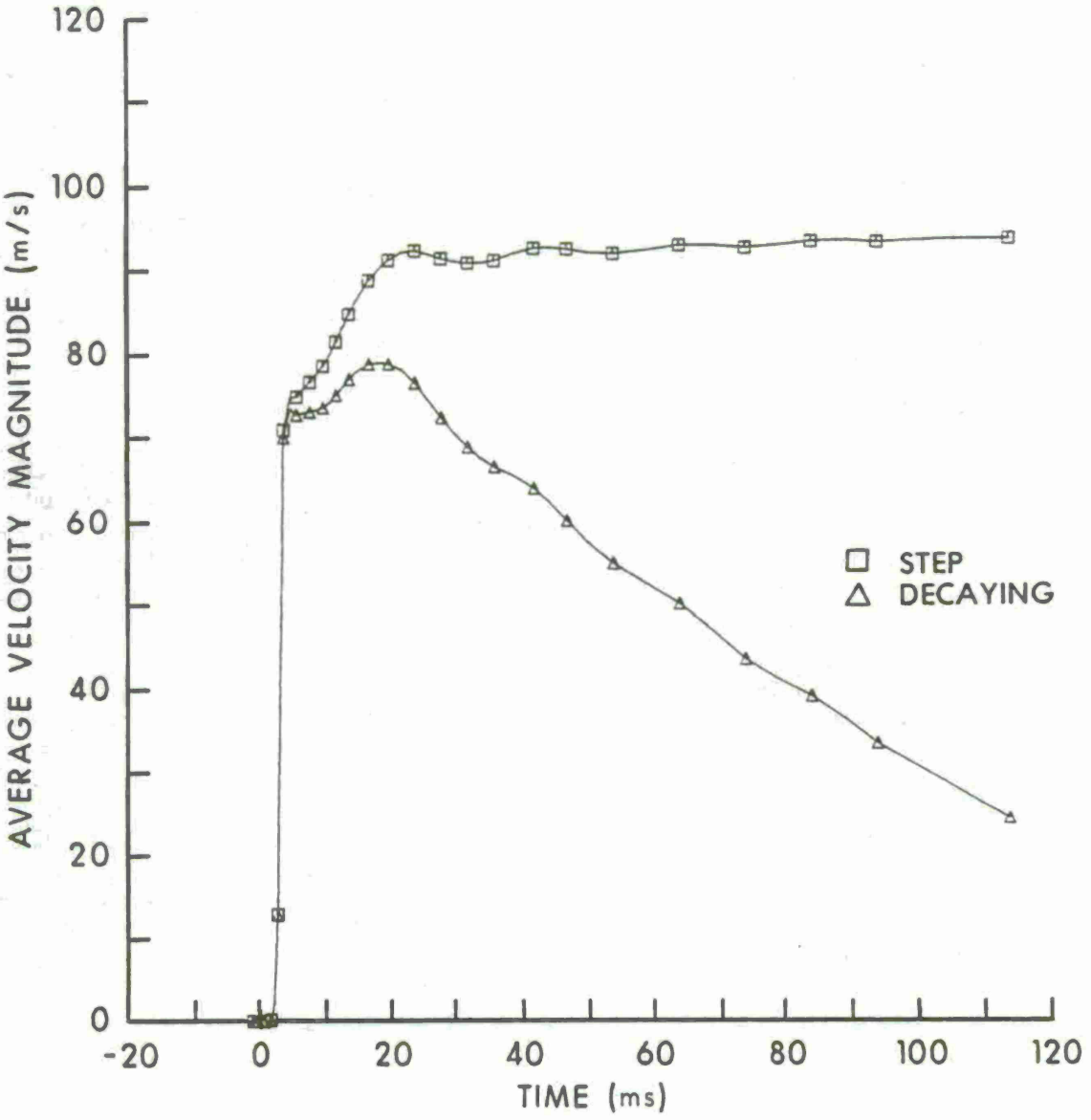

Figure 15. Average magnitude of particle velocity between the cylindrical target and the outer-radial boundary for 34.5 kPa shocks with 20 percent blockage.

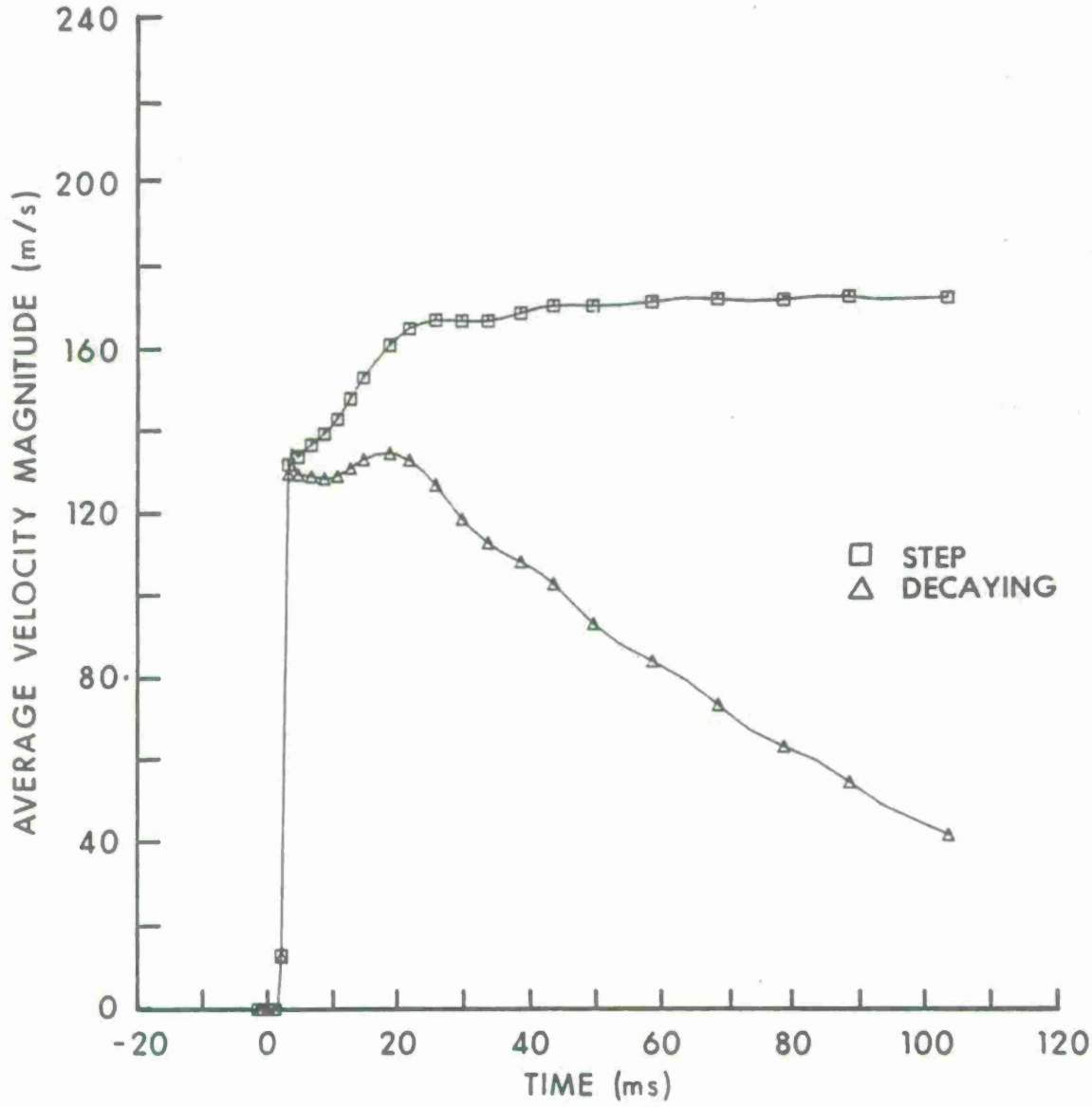

Figure 16. Average magnitude of particle velocity between the cylindrical target and the outer-radial boundary for 68.9 kPa shocks with 20 percent blockage.

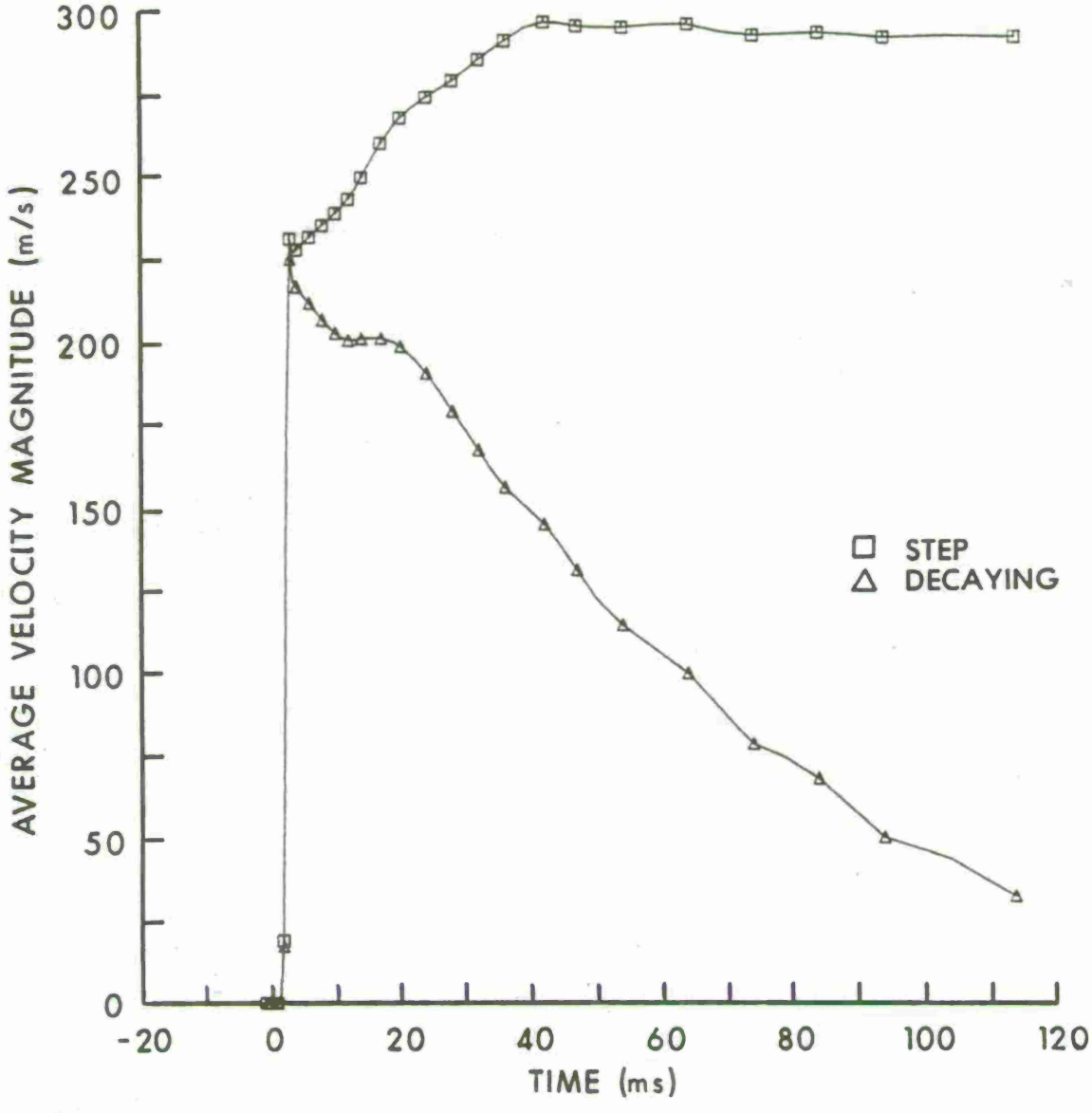

Figure 17. Average magnitude of particle velocity between the cylindrical target and the outer-radial boundary for 137.9 kPa shocks with 20 percent blockage.

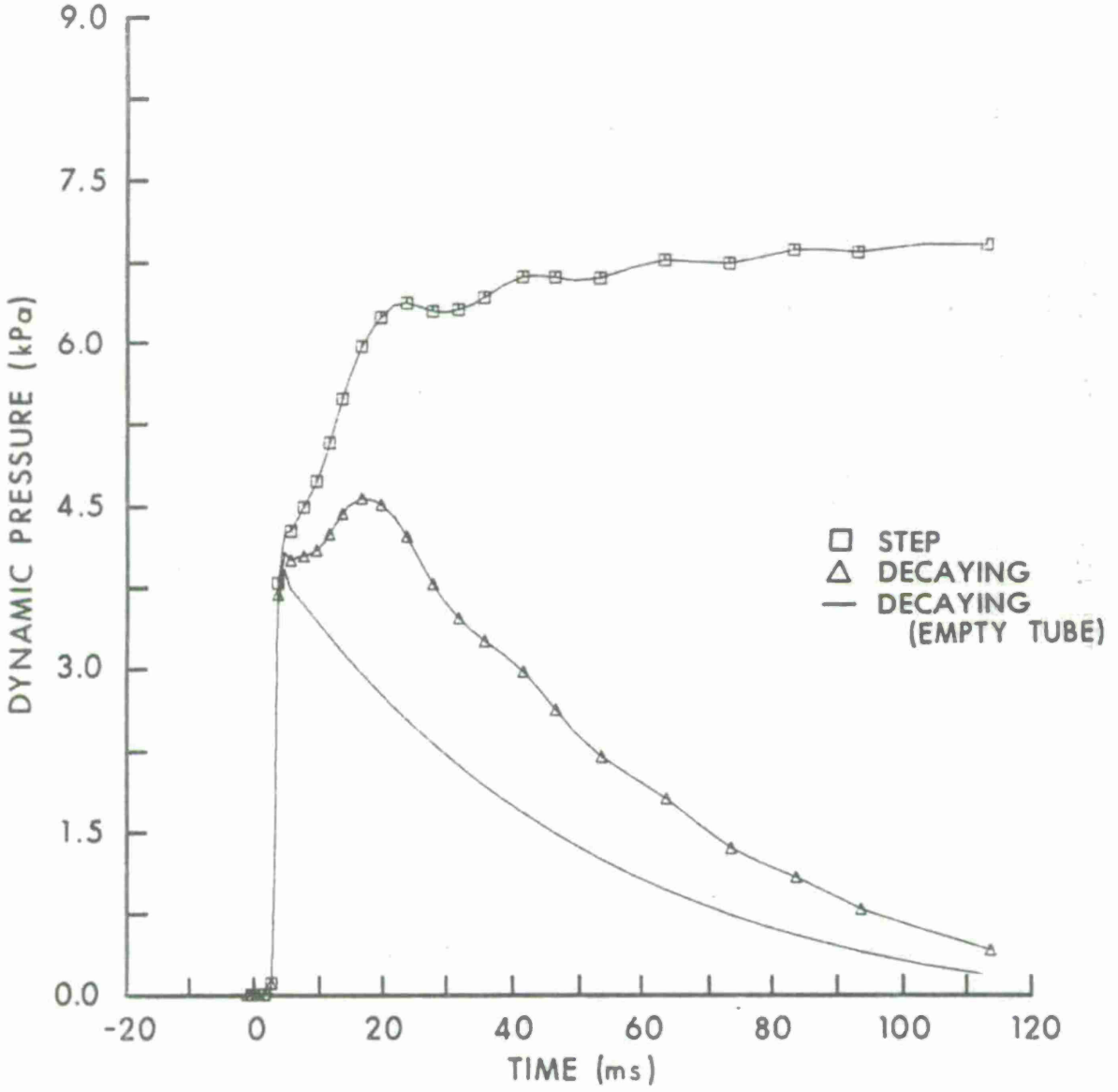

Figure 18. Average dynamic pressure between the cylindrical target and the outer-radial boundary for 34.5 kPa shocks with 20 percent blockage.

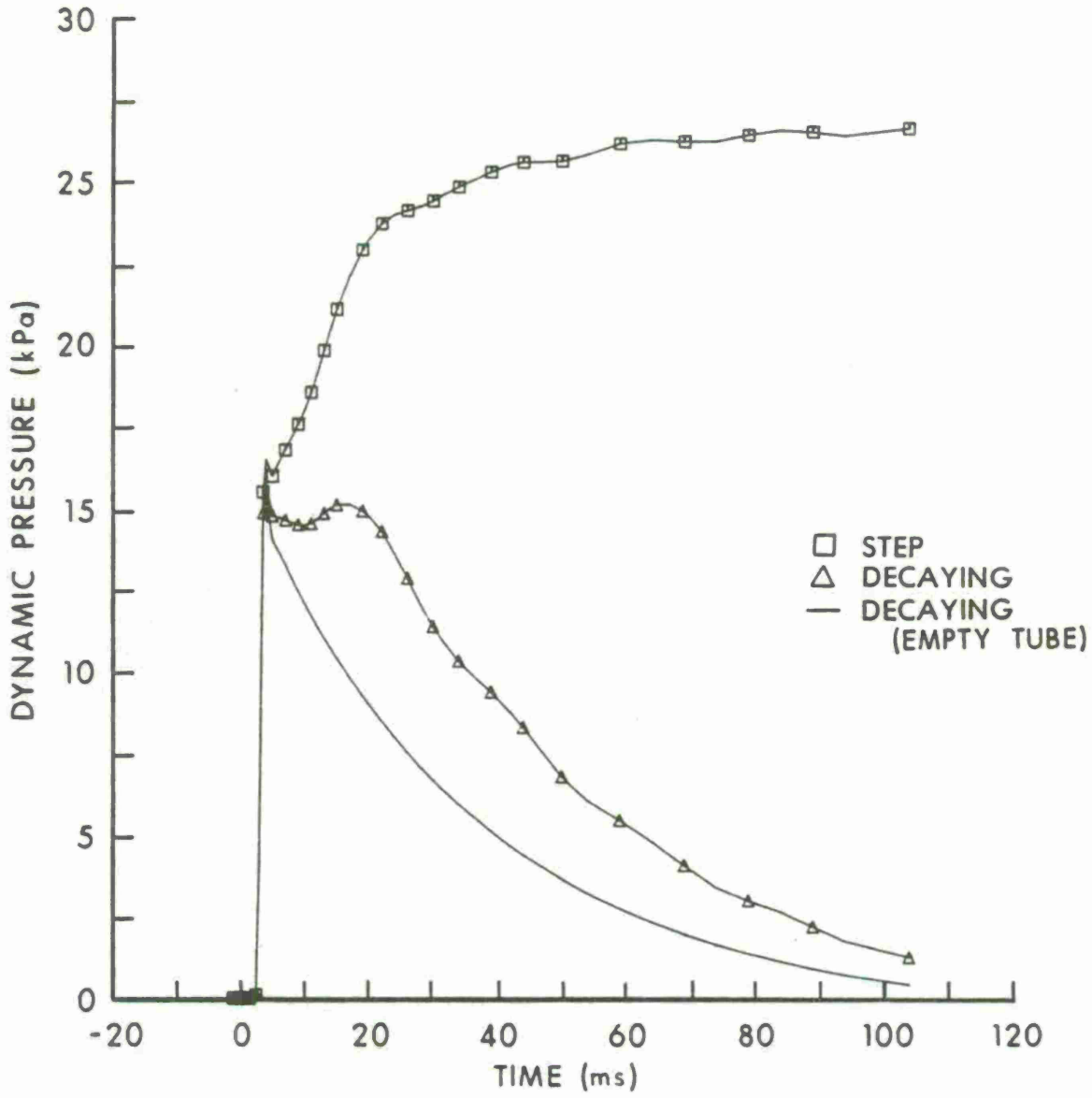

Figure 19. Average dynamic pressure between the cylindrical target and the outer-radial boundary for 68.9 kPa shocks with 20 percent blockage.

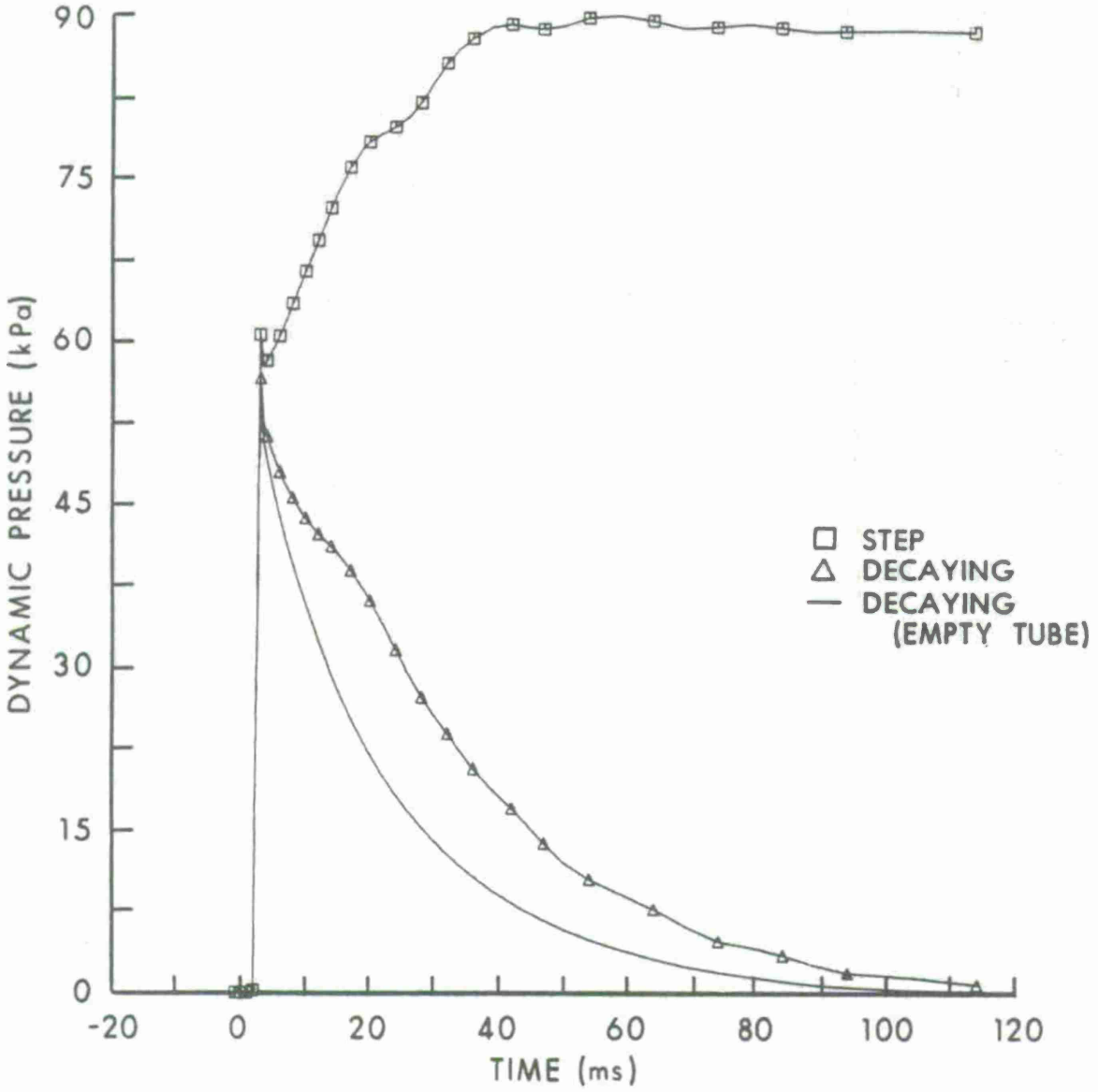

Figure 20. Average dynamic pressure between the cylindrical target and the outer-radial boundary for 137.9 kPa shocks with 20 percent blockage.

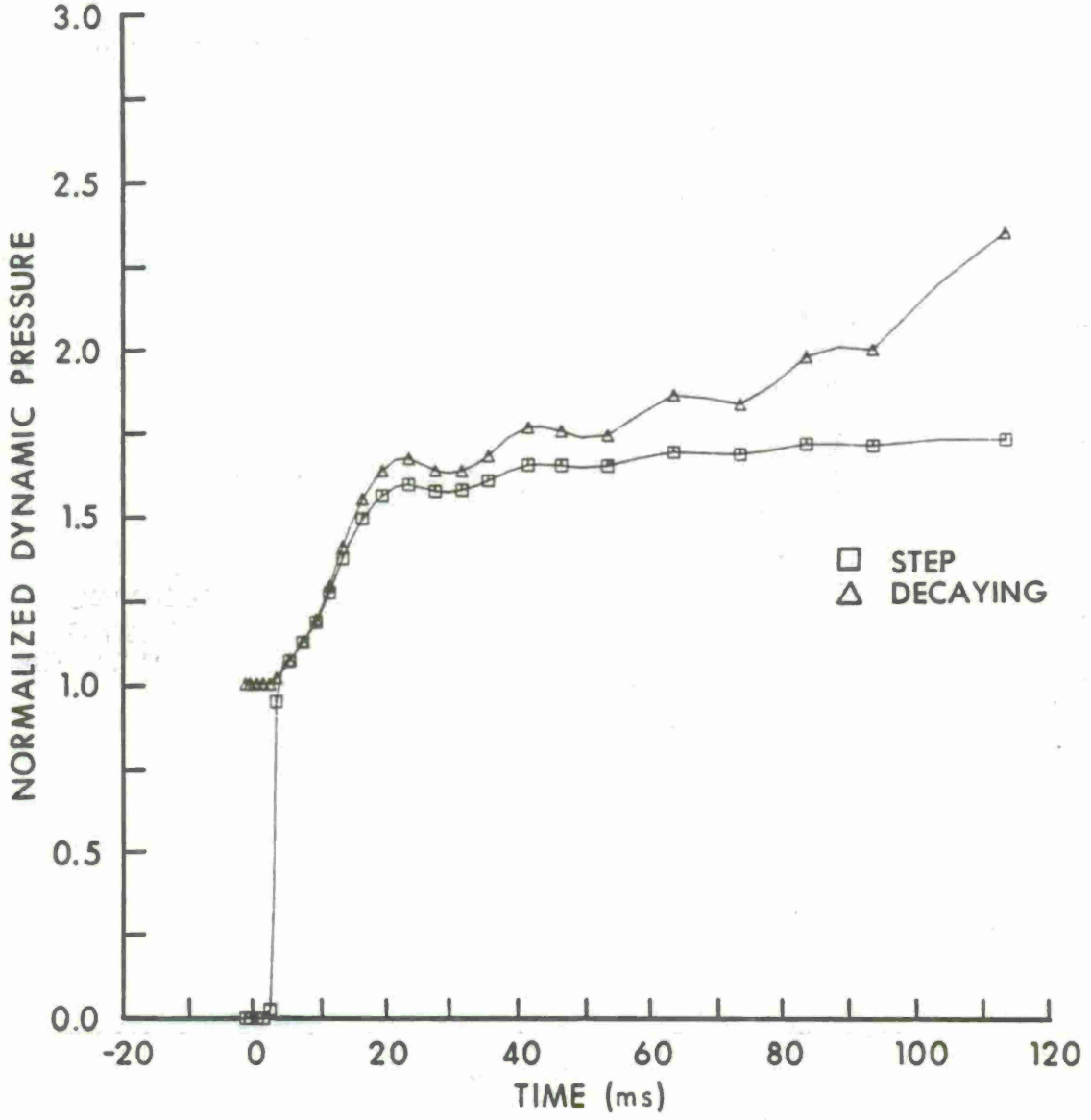

Figure 21. Normalized average dynamic pressure between the target and the outer-radial boundary for 34.5 kPa shocks with 20 percent blockage.

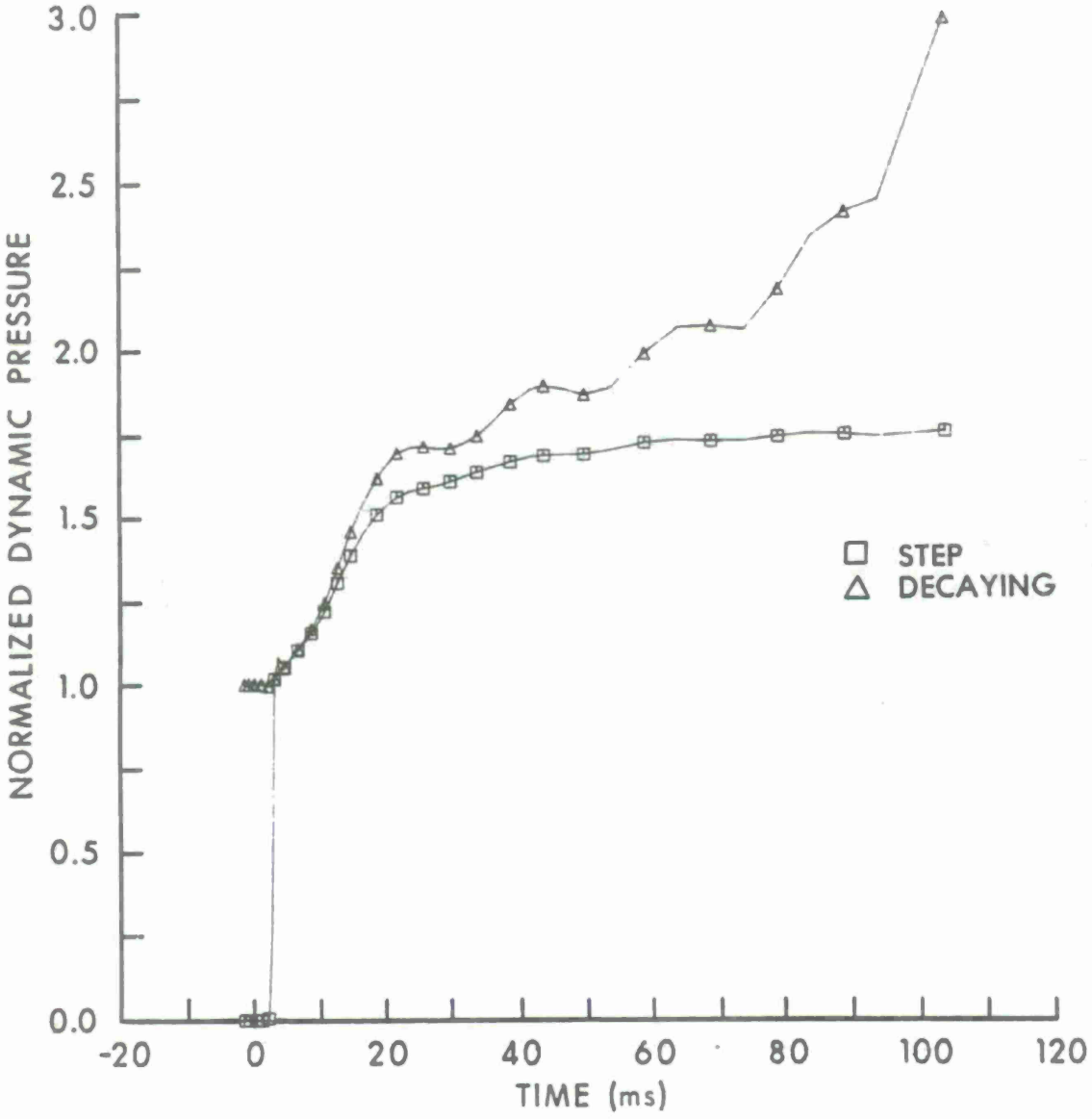

Figure 22. Normalized average dynamic pressure between the target and the outer-radial boundary for 68.9 kPa shocks with 20 percent blockage.

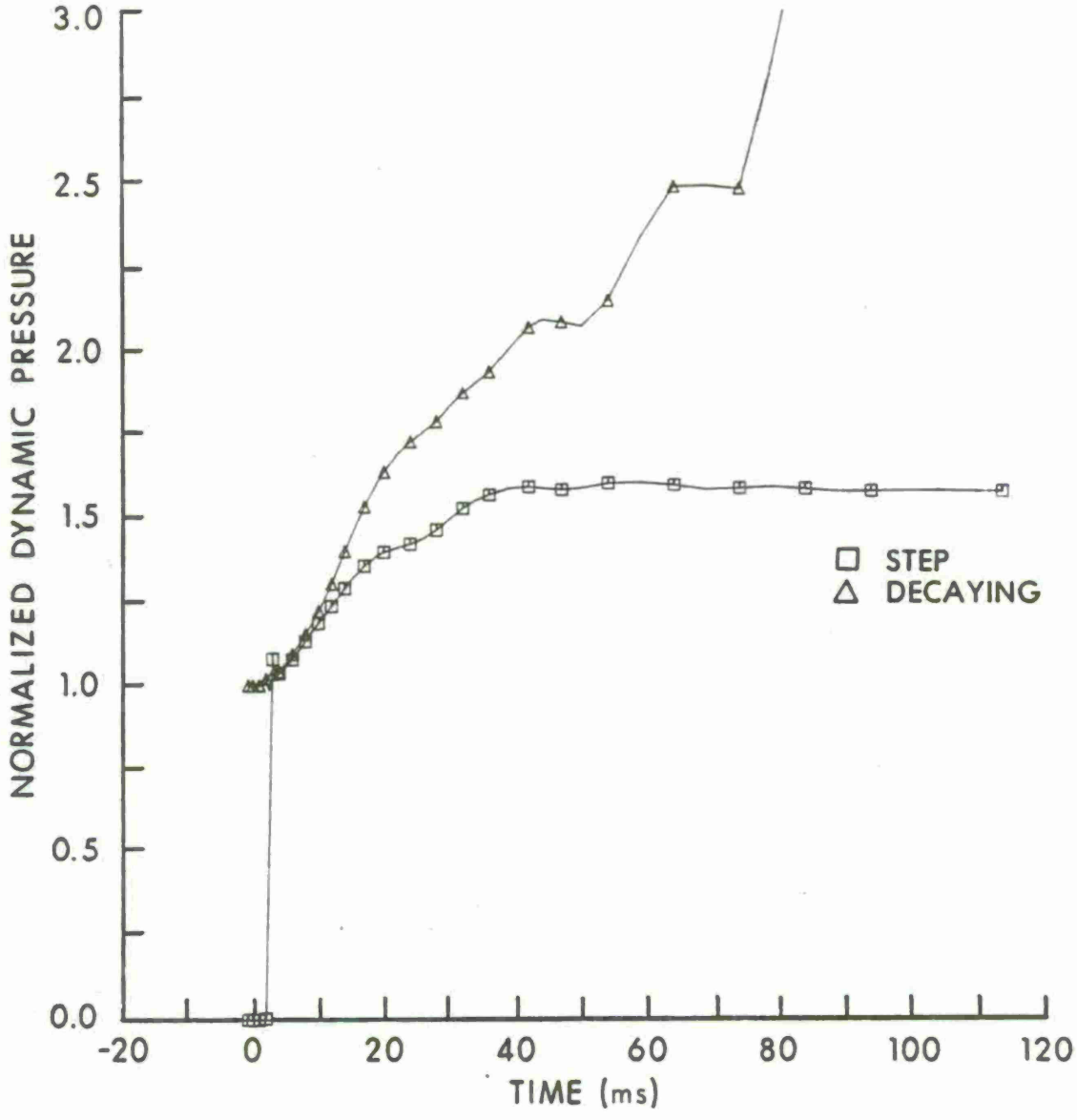

Figure 23. Normalized average dynamic pressure between the target and the outer-radial boundary for 137.9 kPa shocks with 20 percent blockage.

This assumes unchoked flow in the constricted region. This relation was derived to fit the normalized dynamic pressures (Q_B/Q_o) for the step shock at late time in the drag phase. Equation (2) is satisfactory for predicting dynamic pressures in the constricted region for step shocks (which maintained a nearly constant value throughout the drag phase), but is unsatisfactory for use with rapidly-decaying shocks. It gives a marginally satisfactory approximation to the enhanced dynamic pressure at the beginning of the drag phase, but becomes increasingly worse as time progresses. As can be seen in Figures 18, 19, and 20, the dynamic pressures for the decaying shocks become smaller as time progresses. This increases the likelihood of introducing an error when predicting their ratio.

The effective net force for overturning in the drag phase was computed in References 1 and 2 by assuming that the force was directly proportional to the dynamic pressure in the constricted region. For the rapidly-decaying shocks considered in this report, the net axial force on the target becomes negative near the beginning of the drag phase (see Figures 7, 8, and 9). Because the dynamic pressure remains positive, this relation for force is incorrect for the rapidly-decaying shocks considered here, and probably for rapidly-decaying shocks in general.

V. CONCLUSIONS

For the incident shock overpressures considered here, this study of the effect of blockage on loading from rapidly-decaying shocks shows that blockage has much less effect for rapidly-decaying shocks than for step shocks. Loading during the diffraction phase is not affected significantly for either step or decaying shocks. However, unlike the step shocks which showed significant blockage effects throughout the drag phase, the rapidly-decaying shocks showed blockage effects primarily in the early drag phase. Even then, the effects were much less than for step shocks. Except for oscillations due to the reflecting shocks, there is little effect on loading during the rest of the drag phase.

An initially surprising result of this study was that the HULL computations indicated that the net axial force on the target becomes negative shortly after the end of the diffraction phase. This was due primarily to the gradient in the side-on overpressure of the blast wave. This produces a pressure in the plane of the back face which is greater than that at the front face. This (negative) pressure difference is partially compensated for by the drag force exerted on the front face.

Net impulse shows a corresponding decrease from a peak value after the end of the diffraction phase. This is in contrast to net impulse for the step shocks, which increased monotonically.

The flow conditions in the constricted region are enhanced for the decaying shocks. Although the relative enhancement at late time is large

compared with values for the same decaying-shock/target interaction in the free field, it is an enhancement of relatively small values of velocity and dynamic pressure in an absolute sense.

The relation developed in References 1 and 2 for predicting the enhancement of dynamic pressure in the constricted region as a function of blockage ratio for step shocks is not valid for rapidly-decaying shocks. In its present form, its utility is limited to step and slowly-decaying shocks.

The rapidly-decaying planar shock wave used for this study was a mathematical reconstruction of a spherical blast wave predicted by LAMB for a 0.1 KT burst. Because the shock wave in HULL was initially constrained to eliminate its radial divergence and was then constrained to move down a simulated cylindrical tube, it became an increasingly less accurate approximation to a 0.1 KT point-source blast wave as time progressed. This was not important for the present application, because the intent was only to define a rapidly-decaying shock wave for use in the computation. Depending on the application, this expedient method may not be sufficiently accurate if a decaying shock wave for a specific yield and ground range were desired.

REFERENCES

1. N. H. Ethridge, R. E. Lottero, J. D. Wortman, and B. P. Bertrand, "Flow Blockage and its Effect on Minimum Incident Overpressures for Overturning Vehicles in a Large Blast Simulator," Proceedings of the Seventh International Symposium on Military Applications of Blast Simulation, Vol. II, Medicine Hat, Alberta, Canada, 13-17 July 1981.

2. N. H. Ethridge, R. E. Lottero, J. D. Wortman, and B. P. Bertrand, "HULL Hydrocode Computations of Flow Blockage and Its Relation to Overturning of Vehicles in a Large Blast Simulator," (to be published as a BRL Report), US Army Ballistic Research Laboratory, Aberdeen Proving Ground, MD.

3. M. A. Fry, R. E. Durrett, G. P. Ganong, D. A. Matuska, M. D. Stuker, B. S. Chambers, C. E. Needham, and C. D. Westmoreland, "The HULL Hydrodynamics Computer Code," AFWL-TR-76-183, US Air Force Weapons Laboratory, Kirtland Air Force Base, NM, September 1976. (AD #B014070L)

4. J. A. Hasdal, B. S. Chambers, and R. W. Clemens, "Support to BRL: HULL Code Implementation on a CDC 7600," SAI-80-701-AQ, Science Applications, Inc., McLean, VA, August 1979.

5. C. E. Needham and L. A. Wittwer, "The Air Force Weapons Laboratory Low Altitude Multiple Burst (LAMB) Model," AFWL-DYT-75-2 (unpublished).

6. C. E. Needham, M. L. Havens, and C. S. Knauth, "Nuclear Blast Standard (1KT)," AFWL-TR-73-55 (Rev.), US Air Force Weapons Laboratory, Kirtland Air Force Base, NM, April 1975. (AD #A014850)

7. J. D. Wortman, "Blast Computations over a Hemicylindrical Aircraft Shelter,"ARBRL-MR-03115, US Army Armament Research and Development Command, Ballistic Research Laboratory, Aberdeen Proving Ground, MD, July 1981. (AD #B058960L)

8. J. R. Crosnier and J. B. Monzac, "Large Diameter High Performance Blast Simulator," Proceedings of the Fifth International Symposium on Military Applications of Blast Simulation, Stockholm, Sweden, May 23-26, 1977.

9. J. R. Crosnier, S. Gratias, J. B. Monzac, and H. Richard, "Concepts and Design for a Large Diameter High Performance Blast Simulator," Proceedings of the Fourth International Symposium on Military Applications of Blast Simulation, Southend-on-Sea, England, September 9-12, 1974.

DISTRIBUTION LIST

No. of Copies	Organization
12	Administrator Defense Technical Info Center ATTN: DTIC-DDA Cameron Station Alexandria, VA 22314
1	Director of Defense Research & Engineering ATTN: DD/TWP Washington, DC 20301
1	Asst. to the Secretary of Defense (Atomic Energy) ATTN: Document Control Washington, DC 20301
1	Director Defense Advanced Research Projects Agency ATTN: Tech Lib 1400 Wilson Boulevard Arlington, VA 22209
2	Director Federal Emergency Management Agency ATTN: Mr. George Sisson/RF-SR Technical Library Washington, DC 20301
1	Director Defense Intelligence Agency ATTN: DT-2/Wpns & Sys Div Washington, DC 20301
1	Director National Security Agency ATTN: E. F. Butala, R15 Ft. George G. Meade, MD 20755
1	Director Joint Strategic Target Planning Staff JCS Offut AFB Omaha, NB 68113
1	Director Defense Communications Agency ATTN: 930 Washington, DC 20305
9	Director Defense Nuclear Agency ATTN: DDST TIPL/Tech Lib SPSS/K. Goering G. Ullrich SPTD/T. Kennedy SPAS STSP NATD NATA Washington, DC 20305
2	Commander Field Command, DNA ATTN: FCPR FCTMOF Kirtland AFB, NM 87115
1	Commander Field Command, DNA Livermore Branch ATTN: FCPRL P.O. Box 808 Livermore, CA 94550
1	Director Inst for Defense Analyses ATTN: IDA Librarian, Ruth S. Smith 1801 Bearuegard St. Alexandria, VA 22311
1	Program Manager US Army BMD Program Office ATTN: John Shea 5001 Eisenhower Avenue Alexandria, VA 22333

DISTRIBUTION LIST

No. of Copies	Organization
2	Director US Army BMD Advanced Technology Center ATTN: CRDABH-X CRDABH-S Huntsville, AL 35804
1	Commander US Army BMD Command ATTN: BDMSC-TFN/N.J. Hurst P.O. Box 1500 Huntsville, AL 35804
2	Deputy Chief of Staff for Operations and Plans ATTN: Technical Library Director of Chemical & Nuc Operations Department of the Army Washington, DC 20310
2	Office, Chief of Engineers Department of the Army ATTN: DAEN-MCE-D DAEN-RDM 890 South Pickett Street Alexandria, VA 22304
3	Commander US Army Engineer Waterways Experiment Station ATTN: Technical Library William Flathau Leo Ingram P.O. Box 631 Vicksburg, MS 39181
1	Commander US Army Engineering Center Fort Belvoir, VA 22060
1	Commander US Army MERADCOM ATTN: DRDME-EM, D. Frink Fort Belvoir, VA 22060
1	Commander US Army Materiel Development and Readiness Command ATTN: DRCDMD-ST 5001 Eisenhower Avenue Alexandria, VA 22333
1	Commander US Army Armament Research and Development Command ATTN: DRDAR-TDC Dover, NJ 07801
3	Commander US Army Armament Research and Development Command ATTN: DRDAR-LCN-F, W. Reiner DRDAR-TSS (2 cys) Dover, NJ 07801
1	Commander US Army Armament Materiel Readiness Command ATTN: DRSAR-LEP-L, Tech Lib Rock Island, IL 61299
1	Director US Army ARRADCOM Benet Weapons Laboratory ATTN: DRDAR-LCB-TL Watervliet, NY 12189
1	Commander US Army Aviation Research and Development Command ATTN: DRDAV-E 4300 Goodfellow Boulevard St. Louis, MO 63120
1	Director US Army Air Mobility Research and Development Laboratory Ames Research Center Moffett Field, CA 94035

DISTRIBUTION LIST

No. of Copies	Organization
1	Commander US Army Communications Rsch and Development Command ATTN: DRDCO-PPA-SA Fort Monmouth, NJ 07703
3	Commander US Army Electronics Research and Development Command ATTN: DELSD-L DELEW-E, W. S. McAfee DELSD-EI, J. Roma Fort Monmouth, NJ 07703
8	Commander US Army Harry Diamond Labs ATTN: Mr. James Gaul Mr. L. Belliveau Mr. J. Meszaros Mr. J. Gwaltney Mr. F. W. Balicki Mr. Bill Vault Mr. R. J. Bostak Mr. R. K. Warner 2800 Powder Mill Road Adelphi, MD 20783
4	Commander US Army Harry Diamond Labs ATTN: DELHD-TA-L DRXDO-TI/002 DRXDO-NP DELHD-RBA/J. Rosado 2800 Powder Mill Road Adelphi, MD 20783
1	Commander US Army Missile Command ATTN: DRSMI-R Redstone Arsenal, AL 35898
1	Commander US Army Missile Command ATTN: DRSMI-YDL Redstone Arsenal, AL 35898
1	Commander US Army Missile Command ATTN: Technical Library Redstone Arsenal, AL 35898
4	Commander US Army Natick Research and Development Command ATTN: DRDNA-DT, Dr. D. Sieling DRXNE-UE/A. Johnson A. Murphy W. Crenshaw Natick, MA 01762
1	Commander US Army Tank Automotive Rsch and Development Command ATTN: DRDTA-UL Warren, MI 48090
1	Commander US Army Foreign Science and Technology Center ATTN: Rsch & Concepts Br 220 7th Street, NE Charlottesville, VA 22901
1	Commander US Army Logistical Center ATTN: ATCL-SCA Mr. Robert Cameron Fort Lee, VA 23801
3	Commander US Army Materials and Mechanics Research Center ATTN: Technical Library DRXMR-ER, Joe Prifti Eugene de Luca Watertown, MA 02172
1	Commander US Army Research Office P.O. Box 12211 Research Triangle Park NC 27709
3	Commander US Army Nuclear Agency ATTN: ACTA-NAW MONA-WE Technical Library 7500 Backlick Rd., Bldg. 2073 Springfield, VA 22150

DISTRIBUTION LIST

No. of Copies	Organization
1	Commander US Army TRADOC ATTN: ATCD-SA Fort Monroe, VA 23651
2	Director US Army TRADOC Systems Analysis Activity ATTN: LTC John Hesse ATAA-SL, Tech Lib White Sands Missile Range NM 88002
1	Commander US Combined Arms Combat Developments Activity ATTN: ATCA-CO, Mr. L. C. Pleger Fort Leavenworth, KS 66027
1	Commandant Interservice Nuclear Weapons School ATTN: Technical Library Kirtland AFB, NM 87115
1	Chief of Naval Material ATTN: MAT 0323 Department of the Navy Arlington, VA 22217
2	Chief of Naval Operations ATTN: OP-03EG OP-985F Department of the Navy Washington, DC 20350
1	Chief of Naval Research ATTN: N. Perrone Department of the Navy Washington, DC 20360
1	Director Strategic Systems Projects Ofc ATTN: NSP-43, Tech Lib Department of the Navy Washington, DC 20360
1	Commander Naval Electronic Systems Com ATTN: PME 117-21A Washington, DC 20360
1	Commander Naval Facilities Engineering Command ATTN: Technical Library Washington, DC 20360
1	Commander Naval Sea Systems Command ATTN: ORD-91313 Library Department of the Navy Washington, DC 20362
3	Officer-in-Charge Civil Engineering Laboratory Naval Constr Btn Ctr ATTN: Stan Takahashi R. J. Odello Technical Library Port Hueneme, CA 93041
1	Commander David W. Taylor Naval Ship Research & Development Ctr ATTN: Lib Div, Code 522 Bethesda, MD 20084
1	Commander Naval Surface Weapons Center ATTN: DX-21, Library Br. Dahlgren, VA 22448
2	Commander Naval Surface Weapons Center ATTN: Code WA501/Navy Nuclear Programs Office Code WX21/Tech Lib Silver Spring, MD 20910
1	Commander Naval Weapons Center ATTN: Code 3431, Tech Lib China Lake, CA 93555

DISTRIBUTION LIST

No. of Copies	Organization
1	Commander Naval Weapons Evaluation Fac ATTN: Document Control Kirtland Air Force Base Albuquerque, NM 87117
1	Commander Naval Research Laboratory ATTN: Code 2027, Tech Lib Washington, DC 20375
1	Superintendent Naval Postgraduate School ATTN: Code 2124, Technical Reports Library Monterey, CA 93940
1	AFSC (Tech Lib) Andrews Air Force Base Washington, DC 20331
1	ADTC (DLODL, Tech Lib) Eglin AFB, FL 32542
1	AFATL (DLYV) Eglin AFB, FL 32542
1	RADC (EMTLD/Docu Library) Griffiss AFB, NY 13340
1	AFWL/NTES (R. Henny) Kirtland AFB, NM 87115
1	AFWL/NTE, CPT J. Clifford Kirtland AFB, NM 87115
2	Commander-in-Chief Strategic Air Command ATTN: NRI-STINFO Lib Offutt AFB, NB 68113
1	AFIT (Lib Bldg. 640, Area B) Wright-Patterson AFB Ohio 45433
1	FTD (TD/BTA/Lib) Wright-Patterson AFB Ohio 45433

No. of Copies	Organization
1	Director Lawrence Livermore Lab ATTN: Tech Info Dept L-3 P.O. Box 808 Livermore, CA 94550
2	Director Los Alamos Scientific Lab ATTN: Doc Control for Rpts Lib R. A. Gentry P.O. Box 1663 Los Alamos, NM 87544
2	Sandia Laboratories ATTN: Doc Control for 3141 Sandia Rpt Collection L. J. Vortman P.O. Box 5800 Albuquerque, NM 87115
1	Sandia Laboratories Livermore Laboratory ATTN: Doc Control for Tech Lib P.O. Box 969 Livermore, CA 94550
1	Director National Aeronautics and Space Administration Scientific & Tech Info Fac P.O. Box 8757 Baltimore/Washington International Airport MD 21240
1	Aerospace Corporation ATTN: Tech Info Services P.O. Box 92957 Los Angeles, CA 90009
1	Agbabian Associates ATTN: M. Agbabian 250 North Nash Street El Segundo, CA 90245

DISTRIBUTION LIST

No. of Copies	Organization
1	The BDM Corporation ATTN: Richard Hensley P.O. Box 9274 Albuquerque International Albuquerque, NM 87119
1	The Boeing Company ATTN: Aerospace Library P.O. Box 3707 Seatle, WA 98124
1	Goodyear Aerospace Corp ATTN: R. M. Brown, Bldg 1 Shelter Engineering Litchfield Park, AZ 85340
5	Kaman AviDyne ATTN: Dr. N.P. Hobbs (4 cys) Mr. S. Criscione 83 Second Avenue Northwest Industrial Park Burlington, MA 01830
3	Kaman Nuclear ATTN: Library P. A. Ellis F. H. Shelton 1500 Garden of the Gods Road Colorado Springs, CO 80907
1	Kaman Sciences Corporation ATTN: Don Sachs Suite 703 2001 Jefferson Davis Highway Arlington, VA 22202
1	Kaman-TEMPO ATTN: DASIAC P.O. Drawer QQ Santa Barbara, CA 93102
1	Kaman-TEMPO ATTN: E. Bryant, Suite UL-1 715 Shamrock Road Bel Air, MD 21014
1	Lockheed Missiles & Space Co. ATTN: J. J. Murphy, Dept. 81-11 Bldg. 154 P.O. Box 504 Sunnyvale, CA 94088
1	Martin Marietta Aerospace Orlando Division ATTN: G. Fotieo P.O. Box 5837 Orlando, FL 32805
2	McDonnell Douglas Astronautics Company ATTN: Robert W. Halprin Dr. P. Lewis 5301 Bolsa Avenue Huntington Beach, CA 92647
2	The Mitre Corporation ATTN: Library J. Calligeros, Mail Stop B-150 P.O. Box 208 Bedford, MA 01730
1	Pacific Sierra Research Corp ATTN: Dr. Harold Brode 1456 Cloverfield Boulevard Santa Monica, CA 90404
1	Physics International Corp 2700 Merced Street San Leandro, CA CA 94577
1	Radkowski Associates ATTN: Peter R. Radkowski P.O. Box 5474 Riverside, CA 92517
4	R&D Associates ATTN: Jerry Carpenter J. G. Lewis Technical Library Allan Kuhl P.O. Box 9695 Marina del Rey, CA 90291

DISTRIBUTION LIST

No. of Copies	Organization
1	RCA Government Communications Systems 13-5-2 Front & Cooper Streets Camden, NJ 08102
2	Science Applications, Inc. ATTN: Burton S. Chambers John Cockayne P.O. Box 1303 1710 Goodridge Drive McLean, VA 22102
1	Science Applications, Inc. ATTN: Technical Library P.O. Box 2351 La Jolla, CA 92038
1	Systems Science & Software ATTN: C. E. Needham P.O. Box 8243 Albuquerque, NM 87198
1	Systems Science and Software ATTN: Technical Library P.O. Box 1620 La Jolla, CA 92037
1	TRW Systems Group ATTN: Benjamin Sussholtz One Space Park Redondo Beach, CA 92078
2	Union Carbide Corporation Holifield National Laboratory ATTN: Doc Control for Tech Lib Civil Defense Research Proj P.O. Box X Oak Ridge, TN 37830
1	Weidlinger Assoc. Consulting Engineers ATTN: M. L. Baron 110 East 59th Street New York, NY 10022
1	Battelle Memorial Institute ATTN: Technical Library 505 King Avenue Columbus, OH 43201
1	California Inst of Tech ATTN: T. J. Ahrens 1201 E. California Blvd. Pasadena, CA 91109
2	University of Denver Denver Research Institute ATTN: Mr. J. Wisotski Technical Library P.O. Box 10127 Denver, CO 80210
1	IIT Research Institute ATTN: Milton R. Johnson 10 West 35th Street Chicago, IL 60616
1	J. D. Haltiwanger Consulting Services B106a Civil Engineering Bldg. 208 N. Romine Street Urbana, IL 61801
1	Massachusetts Institute of Technology Aeroelastic and Structures Research Laboratory ATTN: Dr. E. A. Witmer Cambridge, MA 02139
2	Southwest Research Institute ATTN: Dr. W. E. Baker A. B. Wenzel 8500 Culebra Road San Antonio, TX 78228
1	SRI International ATTN: Dr. G. R. Abrahamson 333 Ravenswood Avenue Menlo Park, CA 94025
1	Stanford University ATTN: Dr. D. Bershader Durand Laboratory Stanford, CA 94305

DISTRIBUTION LIST

No. of Copies	Organization
1	Washington State University Physics Department ATTN: G. R. Fowles Pullman, WA 99164

Aberdeen Proving Ground

Dir, USAMSAA
ATTN: DRXSY-D
DRXSY-MP, H. Cohen
Cdr, USATECOM
ATTN: DRSTE-TO-F
Dir, USACSL
Bldg. E3516, EA
ATTN: DRDAR-CLB-PA

USER EVALUATION OF REPORT

Please take a few minutes to answer the questions below; tear out this sheet, fold as indicated, staple or tape closed, and place in the mail. Your comments will provide us with information for improving future reports.

1. BRL Report Number _____

2. Does this report satisfy a need? (Comment on purpose, related project, or other area of interest for which report will be used.)

_____

_____

_____

3. How, specifically, is the report being used? (Information source, design data or procedure, management procedure, source of ideas, etc.) _____

_____

_____

4. Has the information in this report led to any quantitative savings as far as man-hours/contract dollars saved, operating costs avoided, efficiencies achieved, etc.? If so, please elaborate.

_____

_____

5. General Comments (Indicate what you think should be changed to make this report and future reports of this type more responsive to your needs, more usable, improve readability, etc.) _____

_____

_____

_____

6. If you would like to be contacted by the personnel who prepared this report to raise specific questions or discuss the topic, please fill in the following information.

Name: _____

Telephone Number: _____

Organization Address: _____

_____

_____